Interplay of downbuilding and gliding in salt-bearing rifted margins: Insights from analogue modeling and natural case studies

Pablo Granado, Pablo Santolaria, and Josep Anton Muñoz

ABSTRACT

Our analogue modeling program simulates a thermally subsiding rifted margin with a regional late synrift to early postrift salt basin. End member models include (1) pure downbuilding in a confined salt basin and (2) dominant gliding on a tilted opened toe margin. The spectrum between these was completed by modeling different amounts of downbuilding versus dominant gliding. Our results provide structural geometries and tectono-stratigraphic architectures for salt structures related to those end member processes, as well as when these occur simultaneously. Downbuilding is represented by vertical aggradation of synkinematic strata, the erosional truncation of megaflaps, and synkinematic debris sourced from salt and prekinematic strata. Dominant gliding is represented by salt-detached extension and related diapirism, resulting in the progressive increase in line lengths of younger stratigraphic units. The transition from downbuilding to dominant gliding is represented by diapir shoulders and the widening of sedimentary depocenters toward flanking salt structures undergoing collapse and salt-detached extension, as well as the truncation of stratigraphy by younger, laterally expanding depocenters. Our modeling results favor the interpretation of an early downbuilding component, followed by gliding for both the South Gabon rifted margin and the Cotiella Basin involved in the south-central Pyrenees fold-thrust belt.

Manuscript received November 30, 2021; provisional acceptance January 25, 2022; revised manuscript received March 19, 2022; revised manuscript provisional acceptance May 4, 2022; 2nd revised manuscript received May 8, 2022; final acceptance May 12, 2022.
DOI:10.1306/08072221203

AUTHORS

Pablo Granado ~ *Institut de Recerca Geomodels, Departament de Dinàmica de la Terra i de L'Oceà, Universitat de Barcelona, Barcelona, Spain; pablomartinez_granado@ub.edu*

Pablo Granado has B.Sc. degrees in geology from the Universitat de Oviedo and the University of Bristol, an M.Sc. degree in tectonics from the Royal Holloway, University of London, and a Ph.D. in structural geology from the Universitat de Barcelona. He is an associate lecturer in structural geology and geodynamics and has worked in Europe, the Americas, and the Middle East. He is the corresponding author of this paper.

Pablo Santolaria ~ *Institut de Recerca Geomodels, Departament de Dinàmica de la Terra i de L'Oceà, Universitat de Barcelona, Barcelona, Spain; pablo.santolaria.otin@gmail.com*

Pablo Santolaria has B.Sc. and M.Sc. degrees in geology and a Ph.D. in geology and geophysics from the University of Zaragoza. He worked as a consultant researcher for the Instituto Geológico y Minero de España (Spanish Geological Survey) until he joined the Geomodels Research Institute in 2017 as a postdoctoral researcher. He is also an associate lecturer at the Universitat de Barcelona.

Josep Anton Muñoz ~ *Institut de Recerca Geomodels, Departament de Dinàmica de la Terra i de L'Oceà, Universitat de Barcelona, Barcelona, Spain; jamunoz@ub.edu*

Josep Anton Muñoz received a Ph.D. in 1985 from the Universitat de Barcelona and worked for the Servei Geologic de Catalunya from 1985 to 1990, when he joined the Universitat de Barcelona. He founded the Geomodels Research Institute in 2007 and was its director until 2017. He is a full professor of structural geology at the Universitat de Barcelona.

ACKNOWLEDGMENTS

This work is a contribution of the Geomodels Research Institute (Universitat de Barcelona).

We acknowledge the financial support of the research project Structure and Deformation of Salt-bearing Rifted Margins (SABREM), PID2020-117598GB-I00, funded by grant no. MCIN/AEI/11.13039/501110011133. This work stems from an industry collaboration with OMV Exploration & Production GmbH through the project "Analogue Modelling of Salt Tectonics" (FBG311629). We are thankful for the constructive reviews of Piotr Krzywiec and Michael Warsitzka and the technical assistance of Oriol Ferrer at the Geomodels Analogue Modelling Laboratory.

INTRODUCTION

In recent years, there has been an increasing understanding of the lithospheric extensional processes that led to the formation of magma-poor, hyperextended rifted margins (e.g., Tugend et al., 2014; Péron-Pinvidic et al., 2019; Chenin et al., 2021; Sapin et al., 2021). On such margins, extensive salt basins can develop during the late thinning of the continental lithosphere before breakup (e.g., Rowan, 2014; Kukla et al., 2018; Epin et al., 2021). Since rock salt is a very weak material and behaves as a fluid over geological time frames (Weijermars and Schmeling, 1986), salt-influenced rifted margins and related minibasins display a large variety of depositional geometries, subsidence rates, and sediment types (Strauss et al., 2021b; Gannaway-Dalton et al., 2022) . However, **Q:2** many studies have focused on the minibasin-flanking structures (e.g., diapirs) and the salt–sediment interaction (Giles and Rowan, 2012; Roca et al., 2021, and references therein) rather than the **Q:3** minibasins themselves. Since minibasins constitute efficient sediment traps (e.g., Pilcher et al., 2011), their stratigraphic architecture can be used as a tool for understanding the underlying mechanisms that govern rift margin evolution, subsidence, and creation of accommodation space (e.g., Gemmer et al., 2004; Granado et al., 2019; Ge et al., 2020; Strauss et al., 2020; Epin **Q:4** et al., 2021; Rowan and Giles, 2021).

Apart from the tectonic subsidence, accommodation space on salt-bearing rifted margins can be generated by stretching the salt and its sedimentary overburden during the gravitational collapse of rifted margins, as well as by differential loading of sediments leading to salt evacuation (e.g., Ge et al., 1997; Brun and Fort, 2004, 2011, 2012; Hudec et al., 2009; Rowan et al., 2012; Peel, 2014; Granado et al., 2016; Jackson and Hudec, 2017; Ge et al., 2020; Figure 1A). Gravitational collapse results in downslope movement/displacement of postsalt sediments along a basal slip surface while internal deformation within sediments and salt takes place. Slipping and internal deformation correspond to gravity-gliding and gravity-spreading mechanisms, respectively (e.g., Ramberg, 1967, 1981; Schultz-Ela, 2001; Peel, 2014). Since combinations of both gliding and spreading are typical in nature, we refer to the process as "dominant gliding" (Figure 1A), which combines components of gliding and spreading (e.g., Schultz-Ela, 2001; Brun and Fort, 2011; Figure 1). Differential loading by sediments can be produced by the progradation of siliciclastic sedimentary systems (Vendeville and Jackson, 1992a; Ge et al., 1997) or by the growth of carbonate platforms (Strauss et al., 2021b). Combinations of gravitational collapse with differential sedimentary loading, as well as extension and salt evacuation across rifted margins, are also known to operate in natural systems (e.g., Granado et al., 2016, 2021; Tavani et al., 2018; Pichel and Jackson, 2020; Roca et al., 2021). Accordingly, subsidence related

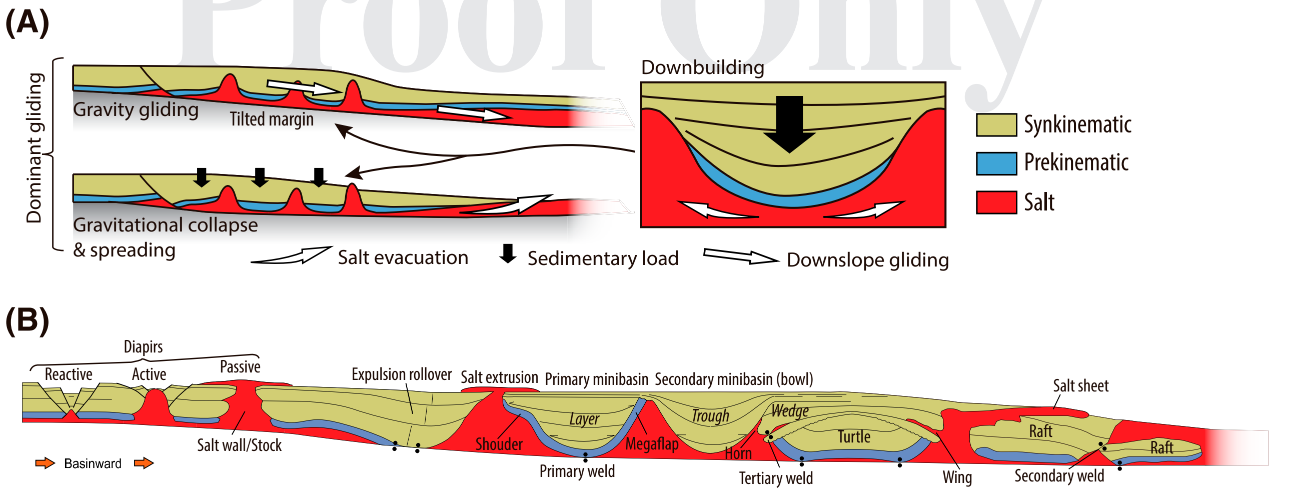

Figure 1. (A) Main gravitational mechanisms that largely govern salt-detached passive margins: gravity gliding and gravity spreading. On a smaller scale, downbuilding controls the formation of minibasins and diapirs. Based on Brun and Fort (2011), Rowan et al. (2012), Goteti et al. (2012), and Peel (2014). (B) Sketched section that illustrates a compilation of salt-related structures and sedimentary sequence geometries used throughout the text.

to salt evacuation during downbuilding and salt-detached extension related to dominant gliding are thus superimposed on the thermal subsidence component of the margin (see Strauss et al., 2021a, b for a recent discussion). The challenge in rifted margin salt–sediment systems therefore resides in constraining the contribution of each of those processes and their timing of activity during margin evolution.

In this paper, we present a series of physical analogue models aimed at testing the contribution of each of the above-mentioned processes. We only show and discuss physical analogue models with differential sediment loading (i.e., vertical and progradational) and a basin slope simulating progressive thermal subsidence on a smoothly stepped presalt topography. Active presalt basement faults have not been included, whereas particular interest has been directed at the shelf, the shelf break, and the transition from slope to distal settings. Our goal was to investigate and to constrain stratigraphic evidence and structural geometries (i.e., diagnostic criteria) to distinguish minibasin and salt structures formed by the contributions of downbuilding and dominant gliding. Our results enlighten interpretations from the offshore South Gabon and the Cotiella minibasins of the southern Pyrenees fold-thrust belt and aid in better understanding the role of salt tectonics processes on both rifted margins and contractional systems that have involved early salt-bearing rifted margins.

SALT TECTONICS TERMS AND DEFINITIONS

In the last several years, salt tectonics jargon has become, frankly, overwhelming (see Hudec and Jackson, 2017). A complete list of terms and definitions is clearly out of the scope of the present work, and the interested reader can make use of the references provided herein. Definitions of the terms used throughout the manuscript are provided below, and illustrated in Figure 1B. The term "minibasin" was introduced by Worrall and Snelson (1989), after the description of sedimentary basins controlled by salt withdrawal (Trusheim, 1960; Vendeville, 2002). Primary minibasins are synkinematic basins largely surrounded by and subsiding into autochthonous salt. Welds are surfaces or zones that join strata originally separated by salt, either autochthonous or allochthonous (Jackson and Cramez, 1989). Primary welds form by the evacuation of autochthonous salt and are typically subhorizontal; secondary welds form by the evacuation of salt from the stem of a steep-sided diapir, whereas tertiary welds form by the evacuation of gently dipping allochthonous salt (Jackson and Hudec, 2017). Primary minibasins may become primary welded at their base after the full (or almost full) evacuation of underlying salt and secondary welded at their lateral boundaries. Secondary minibasins can rest on allochthonous salt or on an equivalent tertiary salt weld, thus lacking the oldest postsalt stratigraphy (e.g., Pilcher et al., 2011; Jackson and Hudec, 2017). It is important to note that minibasin subsidence due to local salt evacuation is independent from the regional basement subsidence (Jackson and Talbot, 1991; Jackson and Hudec, 2017) and that, in fact, both subsidence components need to be taken into consideration (e.g., Strauss et al., 2021a, b).

Salt pillows have a concordant overburden, whereas diapirs cut across their stratigraphic overburden. Diapirs—either stocks or walls—have classically been called reactive, active, and passive (see Vendeville and Jackson, 1992a, b; Rowan and Giles, 2021). Salt wings are wedges of allochthonous salt that protrude from salt diapirs (Lowrie et al., 1991) into their adjacent sediment overburden, and commonly form when diapirs extrude onto the surface to make salt sheets of limited extent during times of erosion, shortening, or reduced sedimentation (Hudec and Jackson, 2017). Salt wings can collapse to form tertiary welds.

Perched flaps and megaflaps are strata upturned to overturned against salt and are commonly associated with diapirs and minibasins (see Callot et al., 2016, Rowan et al., 2016, and Hudec and Jackson, 2017, for details). Salt sheets are constituted by allochthonous salt sourced from a single feeder and emplaced at a stratigraphic level above that of the original (i.e., the autochthonous) salt layer. Turtle structures or turtle anticlines are mounded strata in between diapirs, generally with a flat welded to nearly welded base and a rounded crest affected by oppositely dipping extensional faults. Older stacked sedimentary sequences in turtle structures are thick at their core and thin laterally, whereas younger sedimentary sequences atop their cores are thin, but thicken laterally. Turtle structures form by collapse and subsidence of the flanks of the minibasin (Trusheim, 1960) that could correspond either to the pedestals of the flanking diapirs or the limbs of salt pillows, as a result of regional extension, or in-between salt structures whose minibasins migrate and widen through time. Rafts are fault blocks that have extensionally separated apart and lie entirely on a salt décollement (Duval et al., 1992). Rollovers are formed by strata wedges thickening into listric extensional faults (Hamblin, 1965). Expulsion rollovers result from the removal of underlying salt by the differential sedimentary loading of progradational strata (Ge et al., 1997) and display geometries more akin to progradational clinoforms (Pichel and Jackson, 2020). Sedimentary sequences of multiple kilometers within single minibasins are referred to as wedges, layers, and troughs in regard to the cross-sectional relationship of minibasin strata to flanking diapirs (e.g., Rowan and Weimer, 1998; Rowan and Giles, 2022). Such sequences may occur stacked more or less vertically, expand, or retract depending on the salt–sediment interaction within any single minibasin (e.g., Talbot, 1995; Callot et al., 2016).

ANALOGUE MODELING

Rationale

Our modeling approach has been inspired by observations of several present-day rifted margins (e.g., Granado et al., 2016; Moore and Blanchard, 2017; Chenin et al., 2018; Ge et al., 2020; Sapin et al., 2021; Uranga et al., 2022), as well as fold-thrust belts, where preshortening rifted margin salt tectonics have been interpreted (e.g., McClay et al., 2004; Graham et al., 2012; Harrison and Jackson, 2014; Granado et al., 2019). Most physical analogue modeling studies on salt tectonics have aimed at understanding siliciclastic minibasin systems sinking into salt (see Hudec et al., 2009). On the contrary, comparatively less attention has been paid to the role of carbonates on salt tectonics, although carbonates in the postsalt section of the South Atlantic or the Gulf of Mexico are some but most prospective intervals (Mancini et al., 2001; Snedden and Galloway, 2019; Davison et al., 2021). A striking difference is that carbonate diagenesis results in a rapid increase in density, so that the overburden density exceeds that of salt early on in the burial history. This facilitates early salt evacuation and minibasin subsidence.

Our modeling program has been set up to reproduce elongated structures on map patterns, as inspired by natural examples such as those from Angola (e.g., Ge et al., 2020) or the South Gabon Basin (e.g., Moore and Blanchard, 2017). Classical physical analogue models of rifted margins involving salt tectonics display a rather constant thickness and symmetrical geometry for carbonate rafts (see Brun and Fort, 2004). However, careful inspection of natural examples of raft systems (see, for instance, Duval et al., 1992, or Moore and Blanchard, 2017) clearly shows asymmetric internal geometries, some of which could be compatible with early downbuilding (e.g., thick cores and thinner upturned rims, truncations of oldest stratigraphy against younger stratigraphy), followed by salt-detached rafting and minibasin widening. Those early internal geometries seem to have been systematically neglected and their meaning in terms of salt tectonics initiation disregarded.

EXPERIMENTAL METHODOLOGY

Analogue Materials and Scaling

The models were constructed using modeling materials that are suitable to simulate upper crustal deformation (Weijermars and Schmeling, 1986; Schellart, 2000; Dell'Ertole and Schellart, 2013; Schellart and Strak, 2016; Table 1). Dry well-sorted quartz sand (i.e., 98% pure silica) with an average grain size of 199 µm, a mean coefficient of friction (φ) of 0.6, an average angle of internal friction (ϕ) of 34°, a bulk density of 1500 kg/m^3, and a cohesive strength of ~55 Pa was used (see Ferrer et al., 2017). Sand displays an elastic/frictional plastic behavior, with transient strain hardening before transitioning to stable sliding (e.g., Lohrmann et al., 2003; Adam et al., 2005), being a reasonably good mechanical analog of upper crust brittle rocks. The material used to simulate rock salt was Rhodosil GUM FB (Bluestar Silicones), a transparent viscous polydimethylsiloxane silicone polymer. The density of the silicone polymer at room temperature is 972 kg/m^3, whereas its viscosity is 1.6×11^{-4} Pa·s when deformed at an experimental strain rate of 1.83×11^{-4} cm/s. The silicone polymer behaves as a near-Newtonian fluid, having very low yield strength and a stress exponent n of ~1 at experimental strain rates (Dell'Ertole and Schellart, 2013). Near-Newtonian silicone is considered a reasonable first-order approximation of salt rheology for analogue modeling experiments (Dell'Ertole and Schellart, 2013); however, natural salt behavior is complex and is considered to follow linear-viscous and/or power-law temperature-dependent non-Newtonian rheologies (e.g., Urai et al., 2008; Li and Urai, 2012, 2016; Granado et al., 2021). Hereafter, the term "model salt" is used as a substitute for silicone polymer.

Analogue models were carried out following geometric and dynamic scaling principles, which require driving and resisting forces to be properly related. Geometric scaling guarantees that corresponding ratios of dimensions and angles are comparable between analogue models and nature. The geometric scaling ratio is determined by the procedure for dynamic scaling, which in analogue modeling studies has been established for quite a long time (e.g., Weijermars and Schmeling, 1986; Davy and Cobbold, 1991; Koyi et al., 1993; Vendeville et al., 1995; Wartzika et al., 2015, 2021). This means that 1 cm in our analogue models represents 0.5 km in nature (Table 1). Dynamic scaling requires that trajectories and ratios of acting forces be equal and that the rheological behaviors of the involved materials are similar (e.g., Weijermars and Schmeling, 1986). Therefore, driving and resisting

Table 1. Material Properties and Dynamic Scaling Parameters of the Experimental Program

Parameter	Equation	Model	Nature	Scaling Ratio
Length (L)		1 cm	0.5 km	2×10^{-5}
Density (ρ)				
Sand/brittle rocks		1500 kg/m^3	2567 kg/m^3	0.58
Model salt/decollements		972 kg/m^3	2200 kg/m^3	0.4
Gravity		9.8 m/s^2	9.8 m/s^2	1
Cohesion		55 Pa	50×10^6 Pa	1.1×10^{-5}
Deviatoric stress	$\sigma = \rho \cdot g \cdot L$	121 Pa	1.17×10^7 Pa	1.0×10^{-5}
Ductile layer viscosity		1.6×10^4 Pa·s	10^{18} Pa·s	1.6×10^{-14}
Strain rate	$\varepsilon = \sigma/\eta$			6.5×10^8
Time	$t = 1/\varepsilon$	1 hr	74,000 yr	1.5×10^{-9}
Velocity	$V = L \cdot \varepsilon$	0.5 cm/hr	3.4 mm/yr	1.3×10^4

Scaling ratio refers to the model-to-nature relation of the given magnitude or parameter. Units are given in International System of Units standards.

Proof Only

forces associated with the processes involved in the modeling must be related satisfactorily. In our salt tectonics modeling, driving forces are produced by the vertical loading of sediments, resulting in gravitational buoyancy forces, and by tectonic stresses, resulting in Q:17 lateral pressure forces (Jackson and Hudec, 2007). Resisting forces are caused by the frictional strength of the brittle overburden and by viscous drag at the boundaries of the salt. According to Ramberg (1981), inertial forces are insignificant since strain rates during solid rock flow are very low.

Experimental Setup and Procedure

The experimental setup consists of a rifted margin that displays the transition from the proximal to the distal domain across a necking to hyperextended area, covering shelf, shelf break, and slope settings. The setup includes a confined late synrift to early postrift salt basin (e.g., Rowan, 2014; Figure 2A, B). Then, the modeled margin evolves by seaward tilting representing thermal subsidence following lithospheric thinning, breakup, and accretion of oceanic crust,

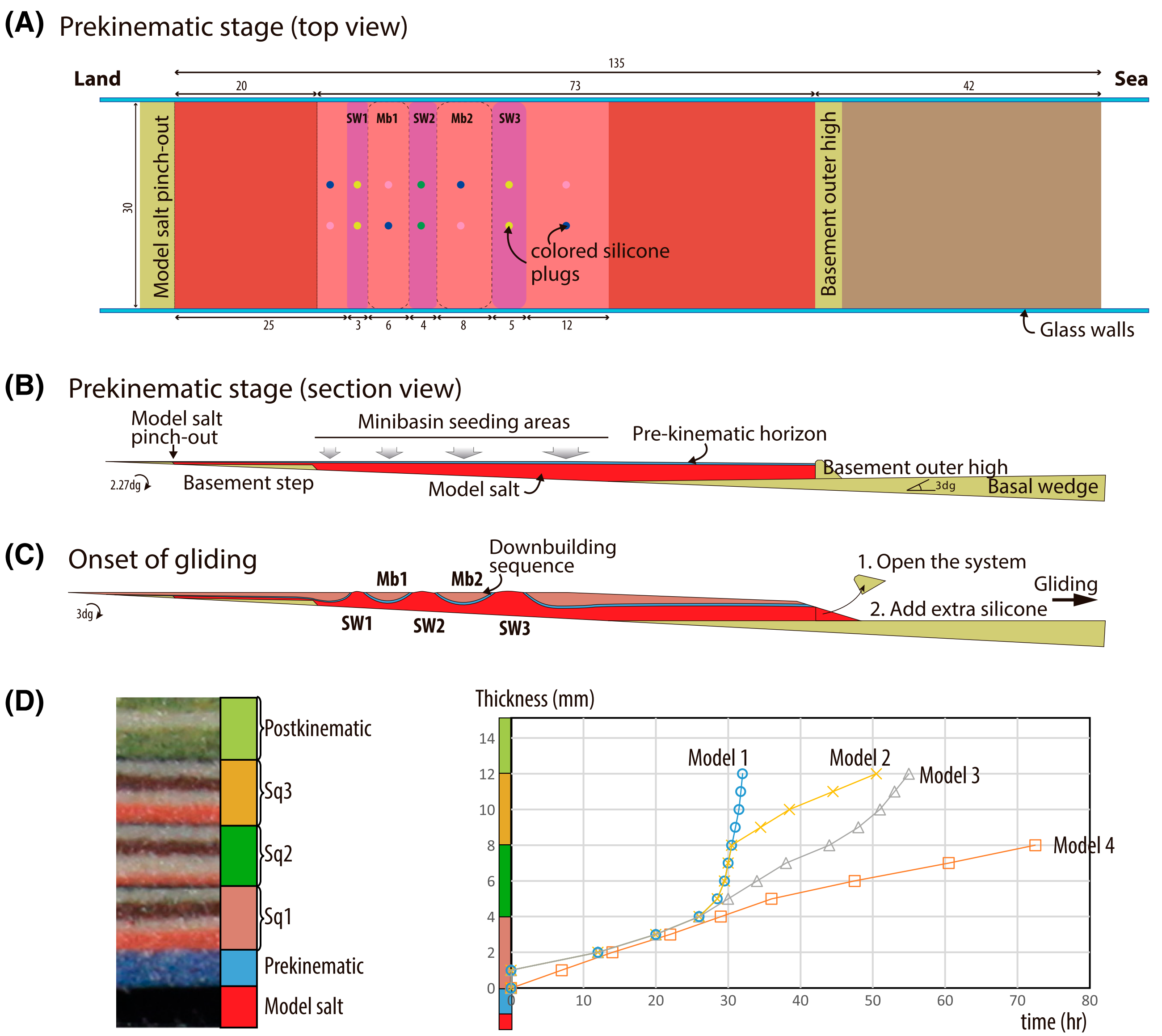

Figure 2. Experimental setup. (A) Plan view showing location and dimensions of key elements of the initial model setup: model salt pinch-out, minibasins (light pink), salt walls (dark pink), and basement outer high (yellow). (B) Cross-sectional view showing the main elements of the model setup at prekinematic stage. (C) Cross-sectional view illustrating the onset of gliding (model 3). (D) Colored sand layers log representing the salt and the pre-, syn-, and postkinematic sequences. A stratigraphic thickness versus time graph represents sedimentation rate curves for each of the analogue models. See text for further details.

such as has been described for magma-poor, hyperextended rifted margins (e.g., Sutra et al., 2013; Chenin et al., 2018; Péron-Pinvidic and Manatschal, 2019). Tilting leads to the gravitational collapse of the model margin, provided the compressional frictional strength of overburden strata at the toe of the slope is overcome (e.g., Rowan et al., 2004), which largely depends on the angle of the basin slope and that of the salt top surface (e.g., Vendeville, 2005). As a result of crustal hyperextension and the slope developed upon necking and thermal subsidence, the initially confined salt basin spills over the outer high and is emplaced basinward as an allochthonous salt sheet (Figure 2C) onto the distalmost margin or even the oceanic crust, Q:19 such as in the Gulf of Mexico (e.g., Hudec et al., Q:18 2013), the South Atlantic (e.g., Aslanian et al., 2009), Q:20 or the North Atlantic (e.g., Adam and Krezsek, 2012).

The used experimental rig consists of two glass Q:21 side walls resting on a basal metal table. The basal table is 170 cm long, 30 cm wide, and 30 cm high (see Figure 2). A strong plastic sheet, undeformable under the modeling conditions, forms the base of the model. The model salt basin is initially confined by a basinward-dipping basement step in the proximal area and a landward-dipping step in the distal area (i.e., a rifted margin outer high) representing a presalt rifted basement topography (Figure 2A, B). These features are built on a 2.3° basinward-tilted basal plate (Figure 2B). Such basal geometry (Figure 2B) produces a tapered model salt basin, which extends for 93 cm from a landward pinch-out to the outer high. The outer high inhibits any initial downslope flow of model salt. The model salt layer is 3 mm thick above the proximal basement step, and beyond this point, it thickens basinward to 23 mm. A blue sand layer overlies the model salt basin. The model salt and the blue layer represent the prekinematic sequence in the modeling program (Figure 2). On top of this sequence, synkinematic layers were poured and have been accordingly labeled as synkinematic sequences 1, 2, and 3 (Sq1, Sq2, and Sq3 in Figure 2D). The synkinematic sequences are made of red, white, brown, and white sand layers. Sequence boundaries are shown by a grain-size-thick black sand marker (Figure 2D). The synkinematic sequences are covered by a postkinematic sequence made of a triplet of green, white, and green sand layers.

During the pouring of synkinematic to postkinematic sequences, a shelf-to-shelf break and slope geometry was built. The shelf break was located 57 cm away from the model salt landward pinch-out. Each of these sand layers was deposited after 0.15° of seaward tilting of the experimental rig, resulting in tapered sand layers whose thickness varies from 1 mm above the model salt pinch-out to 3 mm on the shelf break. Beyond the shelf break, sand was sprinkled on low-lying areas simulating distal margin condensed sequences. The thickness of these layers depended upon the accommodation space created as the salt–sediment system evolved, but were considered to be thin enough to represent pelagic sedimentation. During the experimental evolution program, three structural domains developed: (1) a proximal basin, (2) a minibasin and salt wall province featuring primary minibasins and secondary minibasins (i.e., Mb1 and Mb2 in Figure 2A) flanked by salt walls (SW1, SW2, and SW3, respectively, in Figure 2A), and (3) a distal basin and raft system. Modeled minibasins and salt walls are roughly bidimensional along strike, extending from glass wall to glass wall of the sandbox model, whereas their width progressively increases seaward (Figure 2A–C).

The initiation of model salt evacuation by downbuilding (stage 1) is triggered by pouring the first sand layer on the location of what would be the minibasin depocenters (Figure 2A, C). The uneven distribution of the sand, together with a higher density than the model salt (see Table 1), create a lateral differential loading. Loading triggers minibasins' vertical subsidence while model salt is evacuated from below the minibasin depocenters toward the flanking salt walls. Subsequently, new sand layers were sprinkled away from the minibasin centers, expanding toward the growing salt walls (Figure 2A). The procedure generates outward expanding minibasins from a central seeding horizon, whose three-dimensional (3-D) geometry and aspect ratio conform to elongated minibasins (i.e., throughs, sensu Rowan and Weimer, Q:22 1998 and Jackson et al., 2019; Figure 2C). Minibasins, therefore, sink into a confined model salt.

Gliding (i.e., dominant gliding, sensu Brun and Fort, 2011) of the sand pack is achieved by opening the toe of the salt–sediment system by removing the outer high (Figure 2C). After removing this high, the model salt is no longer confined, thus allowing the salt–sediment system to move seaward and attain cryptic extension (e.g., Vendeville and Jackson, 1992a). The removal of the outer high simulates full lithospheric necking, leading to a margin phase dominated by thermal subsidence (i.e., Sutra et al., 2013; Chenin et al., 2018). Dominant gliding is a continuous process since both the inclination of the deformation rig and the differential loading increase with the deposition of each synkinematic sand layer.

Aiming to test the influence of differential loading versus dominant gliding on geometries and sedimentary record, our experimental program included four models whose evolution is controlled by different amounts of differential loading and dominant gliding (Table 2). Model 1 was carried out by what we here refer to as pure downbuilding (i.e., synkinematic sequences Sq1, Sq2, and Sq3 were deposited under the sole influence of differential loading). Synkinematic sequences Sq1 and Sq2 in model 2 and synkinematic sequence Sq1 in model 3 were also deposited as downbuilding sequences; synkinematic sequence Sq3 in model 2 and synkinematic sequences Sq2 and Sq3 in model 3 were laid upon dominant gliding. All of the synkinematic sequences in model 4 (i.e., Sq1–Sq3) were deposited under dominant gliding conditions exclusively. We emphasize that once triggered, downbuilding continues in our models throughout the experiment and coexists with dominant gliding in models 2 and 3.

Regional subsidence and sedimentation rates are adjusted within geologically reasonable limits for each experiment to favor model salt evacuation and salt wall growth but preclude massive model salt extrusion (i.e., Santolaria et al., 2021). Consequently, regional subsidence and sedimentation rates vary from model to model, as illustrated in the stratigraphic thickness versus time plot (Figure 2D). The sedimentation rate curve for model 1 represents a pure downbuilding evolution of the model salt–sand system fitting to an exponential trend (as recently shown in Santolaria et al., 2021). In contrast, the sedimentation rate curve for model 4 illustrates a dominant gliding process that fits to a linear trend. In between, sedimentation rate curves for models 2 and 3 depart from exponential trends and become roughly linear after the onset of dominant gliding (Figure 2D).

To maintain a record of the experiments during the different phases of modeling, time-lapse high-resolution digital photographs are taken at 90-s intervals from both lateral sides and above the model. At the end of each experiment, model sand packs are longitudinally sectioned at 3-mm spacing and each section is photographed. A 5-cm-wide section along each side of the experiments is systematically discarded to remove any possible border effects.

RESULTS

We show four physical analogue models to illustrate the influence of downbuilding by differential sedimentary loading versus dominant gliding on sedimentary architectures of salt-influenced basins and structural styles (Figures 3, 4). First, we describe in detail the geometries of the minibasins developed, with an emphasis on the cross-sectional geometries of synkinematic strata and their relationships with the prekinematic blue layer, and model salt structures. Second, we describe the geometries of the model salt–sediment interface, and the near-diapir features in terms of strata geometric relationships, erosional relationships, and unconformable relationships. **Q:23** Model salt has been largely evacuated below the minibasins to form salt walls, salt sheets/canopies, welds, primary and secondary minibasins, and related fault families (Figures 3, 4).

Table 2. Summary of the Experimental Program

Model	Onset of Dominant Gliding	Synkinematic Sequence Sq1	Synkinematic Sequence Sq2	Synkinematic Sequence Sq3
1	–	Downbuilding	Downbuilding	Downbuilding
2	Base of Sq3	Downbuilding	Downbuilding	Dominant gliding
3	Base of Sq2	Downbuilding	Dominant gliding	Dominant gliding
4	Base of Sq1	Dominant gliding	Dominant gliding	–

The table includes when dominant gliding started and the main mechanism under which each synkinematic sequence was deposited. Note that downbuilding was a continuous process that coexisted with dominant gliding.

Abbreviations: Sq1–Sq3 = synkinematic sequences 1–3.

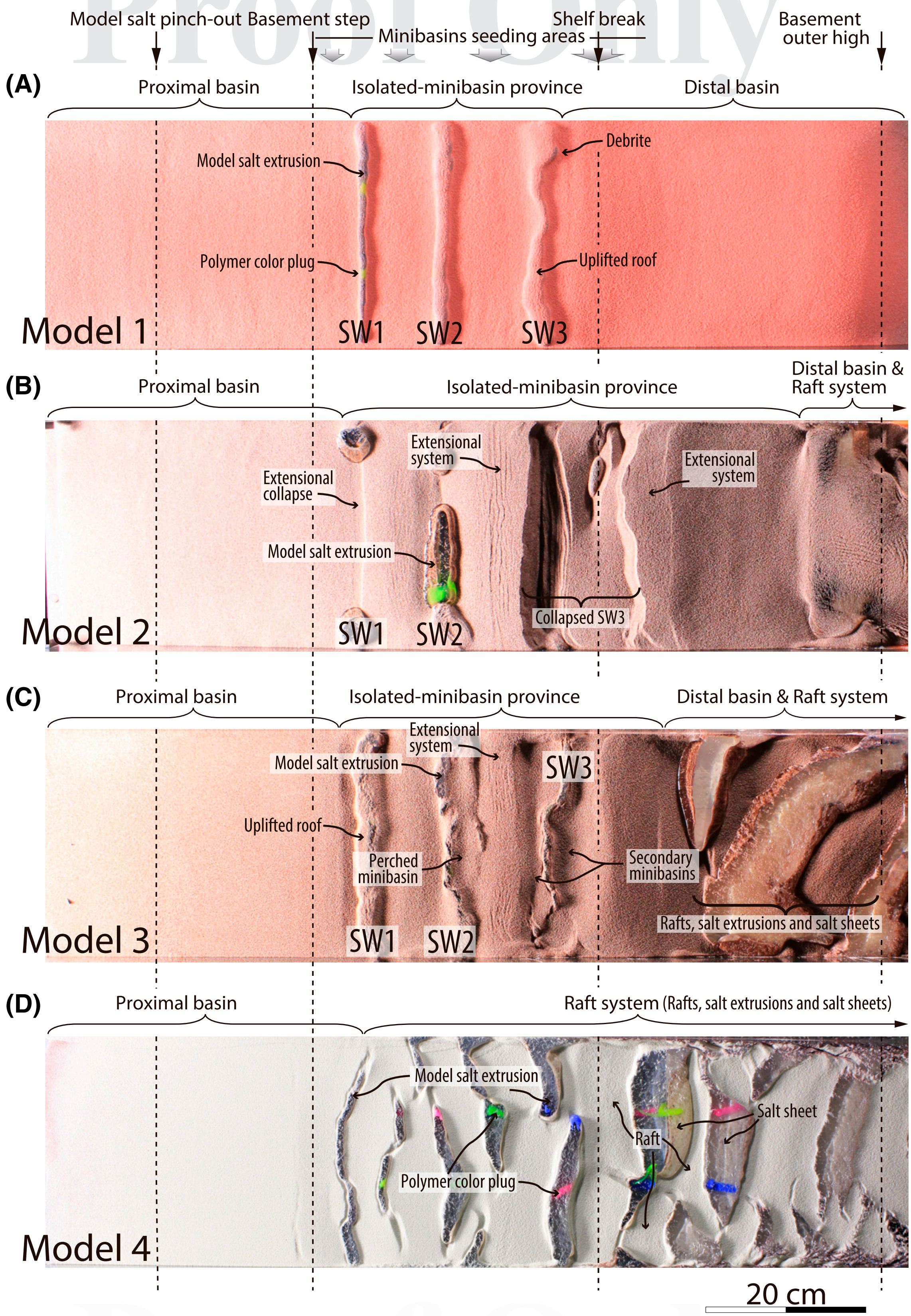

Figure 3. Representative top views of model 1 (A), 2 (B), 3 (C), and 4 (D). Note that top views are not time equivalent; instead, top views of models 2–4 represent the same sedimentary event after the onset of gliding. Key elements of the setup are depicted at the top of the figure.

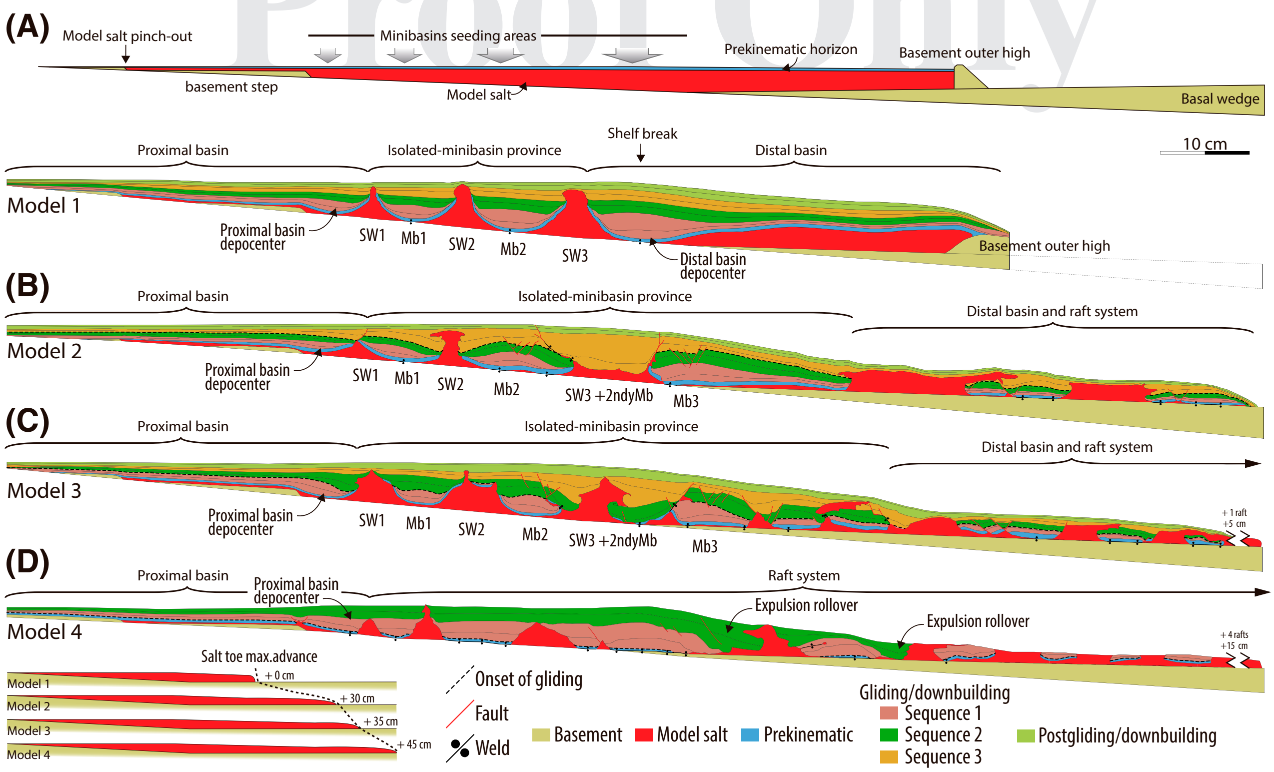

Figure 4. Shape of the original salt basin for reference (A), and representative cross sections of models 1, 2, 3, and 4 (A–D, respectively), which represent the increasing dominance of gliding over downbuilding. Black dashed lines mark the onset of gliding for models 2–4. The distalmost part of models 3 and 4 has been removed for visualization purposes. A comparative sketch portraying the maximum advance of the salt toe is shown in the bottom right corner.

Downbuilding Model (Model 1)

Model 1 was built in a confined model salt system, with two central minibasins (i.e., Mb1 and Mb2), a proximal basin, and a distal basin beyond the shelf break (Figure 4A). Note that we do not refer to the proximal and distal basins as minibasins, since those are not largely surrounded by salt and thus do not fall within the original definition of minibasins. Model 1 accommodated three downbuilding synkinematic sequences. Three salt walls and a distal salt plateau beyond the shelf break developed (Figure 4A; Table 2). The three salt walls occur as linear features, with a positive relief at the model surface (Figure 3A). The minibasins Mb1 and Mb2 and the depocenters of the proximal and distal basins are characterized by a folded prekinematic layer at their base. The prekinematic layer is onlapped by synkinematic sequences 1 and 2. Model salt extruded to the surface at the end of synkinematic sequence Sq2, whereas synkinematic sequence 3 shouldered the extruding salt (Figure 4A). The two minibasins are symmetric and display a bowl geometry in cross section, whereas their 3-D geometry conforms to elongated minibasins. The two external basins (i.e., proximal and distal), however, displayed a subtle tilting; although the proximal is tilted seaward, the distal basin is tilted landward (i.e., toward SW1 and SW3, respectively). Seaward from the shelf break, the distal basin on the model salt is characterized by a condensed synkinematic succession. The thinning of each synkinematic sequence decreases upward, revealing that the amount of downward flow of the model salt and related thickening was reduced progressively as salt was evacuated underneath the minibasin and welding approached. It should be noted that model salt slightly flowed over the outer high during downward flow and thickening.

Downbuilding Followed by Late Dominant Gliding (Model 2)

Model 2 accommodated two downbuilding synkinematic sequences, followed by a third sequence deposited during dominant gliding conditions

(Figures 3B, 4B). Model 2 displays a proximal basin, flanked seaward by an extensional collapse fault with an incipient salt roller immediately beyond the proximal basement step. Three primary minibasins were flanked by passive salt walls, and a secondary minibasin developed after the collapse of SW3 at the shelf break. Minibasin 2 features a turtle geometry (Figure 4B). The secondary minibasin displays a bowl-type cross-sectional geometry, and forms a sediment depocenter nearly similar in size to the primary minibasin 2, but **Q:25** lacks the oldest stratigraphy. Salt wall SW2 and the secondary minibasin display strong changes in geometries and model salt–sediment relationships along strike. The extruded model salt in SW2 grades laterally into a stretched overburden, whereas the collapse of SW3 assisted by synkinematic sedimentation led to a continuous secondary minibasin that is locally pierced by the model salt (Figure 3B).

Model 2 also displays a distal domain in which rafts and salt sheets occur (Figure 4B). As a result of the component of dominant gliding, the geometries of minibasins and related salt structures in model 2 strongly differ from those of model 1. Salt-detached extension during dominant gliding was accommodated by the widening and collapse of salt walls (Vendeville and Jackson, 1992a), favored by coeval synkinematic sedimentation. Turtle anticlines and a secondary minibasin resulted from this process, in contrast with model 1, where none of these structures were developed since only pure downbuilding was included. The salt walls in model 2 are comparatively shorter than those of model 1. The primary minibasins in model 2 display larger basal welds, whereas in model 1 the basal welds are narrower and positioned exactly below the central parts of the minibasins. The welds in the model 2 minibasins are comparatively larger and wider, resulting from the collapse of the salt walls and the formation of turtle structures.

Downbuilding Followed by Early Dominant Gliding (Model 3)

Model 3 was built with one synkinematic sequence of downbuilding, followed by two synkinematic sequences laid during dominant gliding (Figures 3C, 4C). Geometries of minibasins and related salt structures strongly differ from those of model 1 as well and are characterized by a larger number of near-diapir structural features than those of model 2. A larger number of rafted blocks developed in model 3. Model 3 displays a minibasin and salt wall province similar to that in model 2, but with wider salt walls and larger diapir shoulders, including a secondary minibasin developed during the collapse of SW3. The secondary minibasin is flanked by and laterally welded to the adjacent primary minibasins, such as in model 2. The secondary minibasin consists of two wedges that expand into the remnants of the collapsed SW3 (Figure 4C), and contrary to model 2, it contains at its base the oldest postsalt stratigraphy. The distal rafts and salt sheets in model 3 (Figure 4C) evolved from initially linear features perpendicular to the gliding direction to oblique structures, as observed in the top view photographs, hence indicating vertical axis rotations (Figure 3C). Secondary and tertiary welds are also recognizable (Figure 4C). As in model 2, extension related to dominant gliding led to lateral changes on the geometry of salt walls and sand packages, mainly affecting the linearity of salt extrusions and the appearance of diapir shoulders (i.e., SW2 and SW3; Figures 3C, 4C). Since dominant gliding was an early process (i.e., earlier than that for model 2), it had a larger effect on the model evolution.

Dominant Gliding Model (Model 4)

Model 4 was built exclusively under dominant gliding (Figures 3D, 4D) and accommodated two synkinematic sequences (Figures 3D, 4D). Model 4 consists of up to nine salt walls and a distal salt sheet domain (Figure 3D), along with several rafts (Figure 4D). Collapsed salt walls beyond the shelf break evolved into expulsion rollovers (Figure 4D). Expulsion rollovers prograde basinward and fill in the gap between raft blocks. All of the features above are indicative of thin-skinned salt-detached extension coeval with salt evacuation as a result of the progradational sedimentary loading. In model 4, only two synkinematic sequences were added before the rafts welded at the model salt base, preventing further gravity gliding; this is a main difference from the other models.

Model 4 illustrates a complete suite of salt-related structures, which display the salt–sediment evolution through space and time, with younger, less evolved diapirs located landward, and far more developed, earlier structures located basinward (Figure 4C). The landwardmost diapir structure immediately above the basement step is bounded by inward-dipping conjugate extensional faults formed during the initial reactive stage, as the prekinematic layer was stretched, faulted, and eventually pierced (e.g., Vendeville and Jackson, 1992b). The next diapir located seaward is buried by synkinematic strata, but can be classified as passive since the model salt reached the model surface soon after its active stage (Rowan and Giles, 2021). Basinward, the salt structures are far more evolved, showing evidence for passive rise, with salt wings and perched flaps and shoulders, and the collapse in the form of a seaward-advancing expulsion rollover, rafts with collapsed wings in the form of tertiary welds, and salt sheets and canopies locally overlaid by synkinematic sediments resting on tertiary welds (Figures 3D, 4D). At the surface, the model salt–sediment system is characterized by a more irregular structural pattern than in previous models, with a dominant gliding component (Figure 3D). For instance, rafts have variable dimensions and aspect ratios and shapes in top view, whereas reactive diapirs and salt walls are relatively linear features whose width decreases landward. This suite of structures shows that salt-detached extension migrated upslope with time.

Structural Geometries and Tectono-stratigraphic Architecture

We present in the following a detailed comparison of the minibasins developed in each model to illustrate our results and decipher the effect of downbuilding and dominant gliding on both sedimentary architectures and structural geometries (Figure 5). We have also selected a series of examples to illustrate near-diapir features (Figures 6–8). We describe and compare the model minibasins from the proximal to the distal sectors, together with near-diapir features associated with salt evacuation. Q:26

In all four models, the proximal basin developed with a progressive basinward tilt over the basement step, landward of the first salt wall

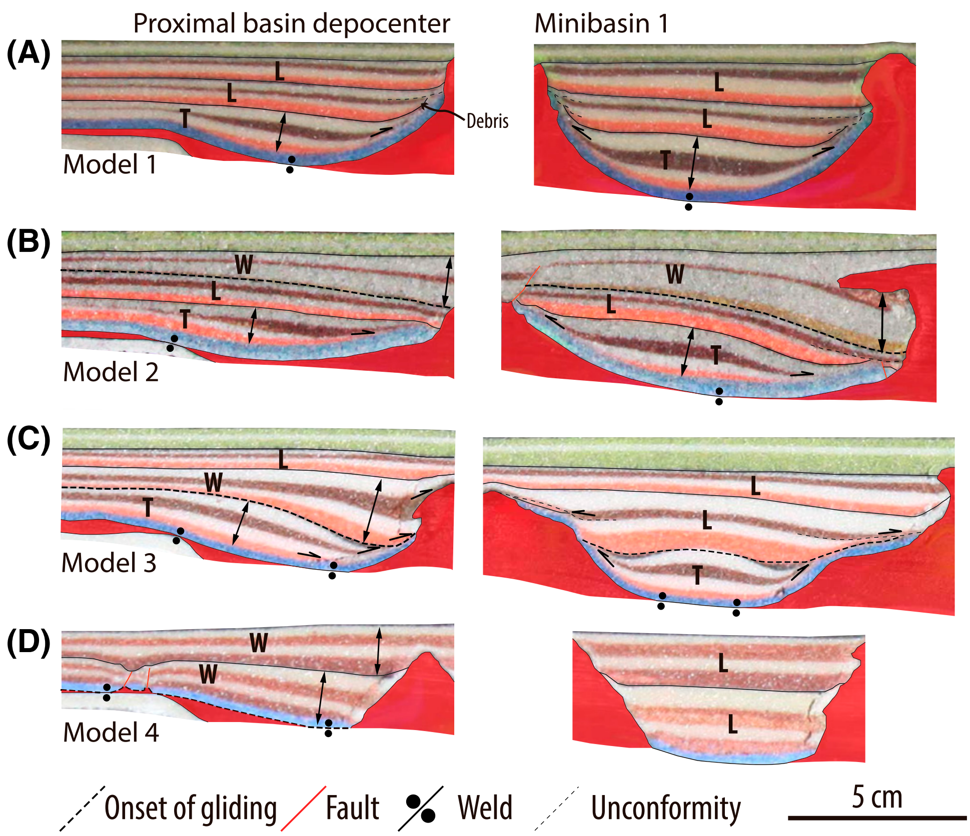

Figure 5. Detailed view and interpretation of the proximal basin (left) and minibasin 1 (right) of models 1–4 (A–D, respectively). Model 4 does not include downbuilding, and the depocenters correspond to those developed on a position equivalent to that of proximal basin and minibasin 1 for models 1–3. Tectono-stratigraphic packages constituting minibasins are described and labeled after Rowan and Weimer (1998) and Rowan and Giles (2023). L, T, and W refer to layer, trough, and wedge tectono-stratigraphic architectures, respectively.

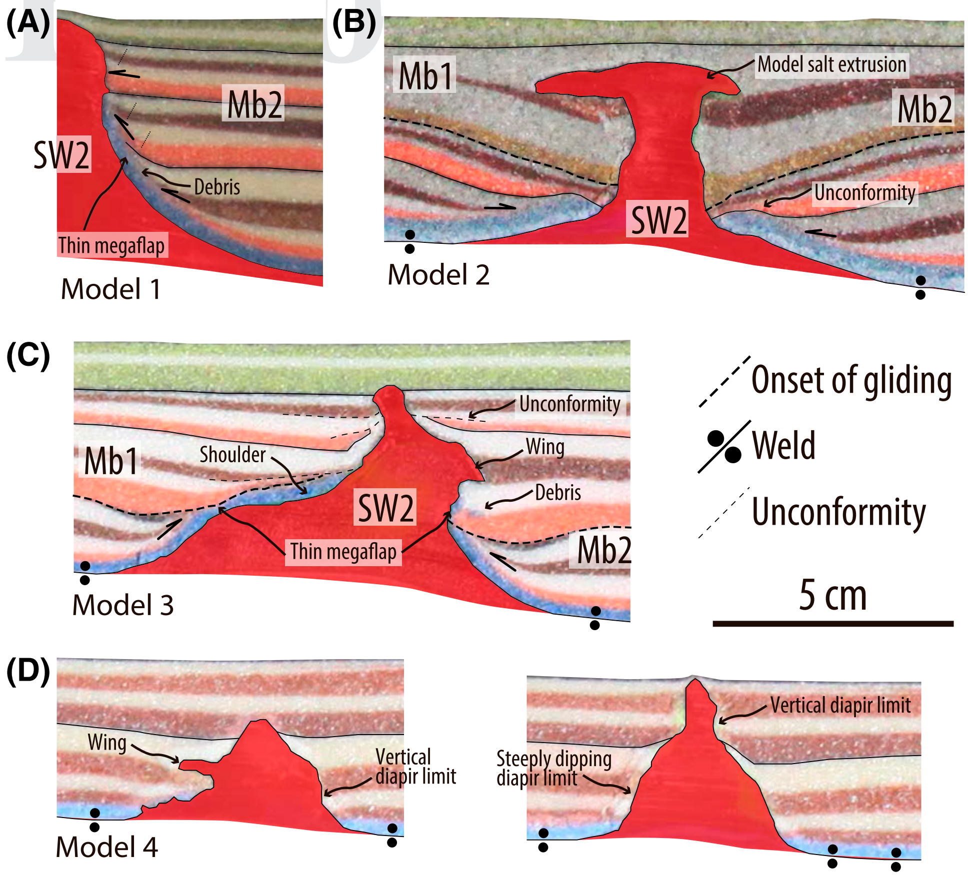

Figure 6. Close-ups and interpretation of near-diapir features flanking salt wall 2 (SW2) in models 1 (A), 2 (B), and 3 (C). (D) Profiles of the same salt wall at different positions along strike, developed at the same position as SW2 in the other models (see Figures 3 and 4 for reference). Mb1 and Mb2 = minibasins 1 and 2.

(i.e., SW1; Figure 5). The observed different geometries for the proximal basins in the four models are correlated with the transition from pure downbuilding to dominant gliding mechanisms. In models with initial downbuilding (i.e., models 1–3; Figure 5A–C), the internal geometry of the synkinematic sequences Q:27 in the proximal basin is that of throughs. The younger synkinematic sequences lap seaward on the prekinematic layer and either thin or lap landward on the prekinematic sequences. Younger synkinematic sequences in the proximal basin unconformably lay over previous layers and either abruptly end against or cover SW1 (Figure 5). On the contrary, upon dominant gliding exclusively (i.e., model 4), the prekinematic layer, basinward of the basement step, shows an abrupt truncation against the flanking salt wall without bending; this break corresponds to an extensional fault produced during the initial reactive stage of the diapir. Landward, immediately above the basement step, conjugate extensional faults formed (Figure 5D) and laterally evolved into a reactive diapir (e.g., Vendeville and Jackson, 1992b), as shown by the top view image (Figure 4D). The earliest synkinematic layers in the proximal basin of model 4 also die out abruptly onto the model salt, whereas the younger ones on top first conform to expanding, seaward-thickening wedges (Figure 5D). To summarize, differences in the geometry of the synkinematic sequences of the proximal basin relate to the dominant mechanism (i.e., downbuilding versus gliding); troughs developed during downbuilding, particularly at the earlier stages characterized by high rates of salt evacuation, whereas wedges develop if the dominant mechanism is gliding. Layers formed indistinctively during periods of decreasing salt evacuation.

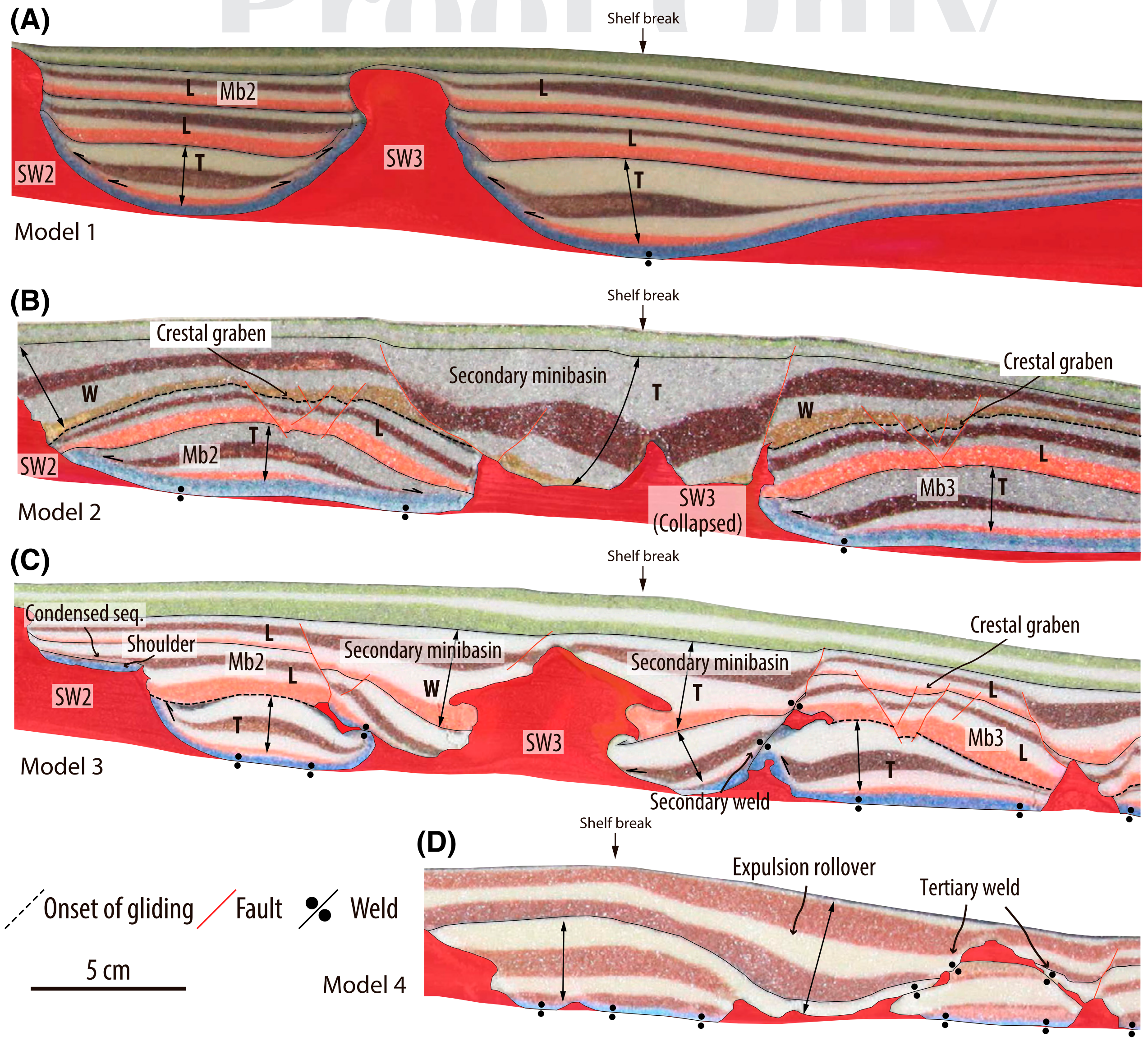

Figure 7. Close-ups and interpretation of minibasins 3 and 4 (Mb3 and Mb4) and related structures (i.e., collapsed salt walls and secondary minibasins) of models 1 (A), 2 (B), 3 (C), and 4 (D). Note the expulsion rollover developed at the equivalent position to salt wall 3 (SW3) in the other models. The expulsion rollover developed as a counterregional structure and shows geometries compatible with extension but also with basinward salt evacuation. L = layer architecture; Seq. = sequence; T = trough architecture; W = wedge tectono-stratigraphic architecture. Q:59

In all four models, Mb1 shows marked differences in structural geometries and tectono-stratigraphic architecture (Figure 5). One main difference with the proximal basin is that Mb1 (and Mb2) are flanked on either side by salt walls, whereas the proximal basin only has one flanking salt wall (Figure 4). In model 1, Mb1 is largely symmetrical (Figure 5A), with a folded prekinematic layer welded at its central position, and forming megaflaps that thin upward (Figure 5A). Thinning of the megaflaps is most likely due to the erosion of steep-sided diapirs roofs by the granular flow of the prekinematic layer, rather than stretching of the layer. In this sense, the time of salt extrusion and piercing of the prekinematic layer in Mb1 is marked by the presence of sand debris from the prekinematic blue sand redeposited on the peripheral synclines within the youngest layer of the synkinematic sequence 1 (Figure 5A). Internally, synkinematic sequence 1 corresponds to a through, whereas Q:28 the following synkinematic sequences conform

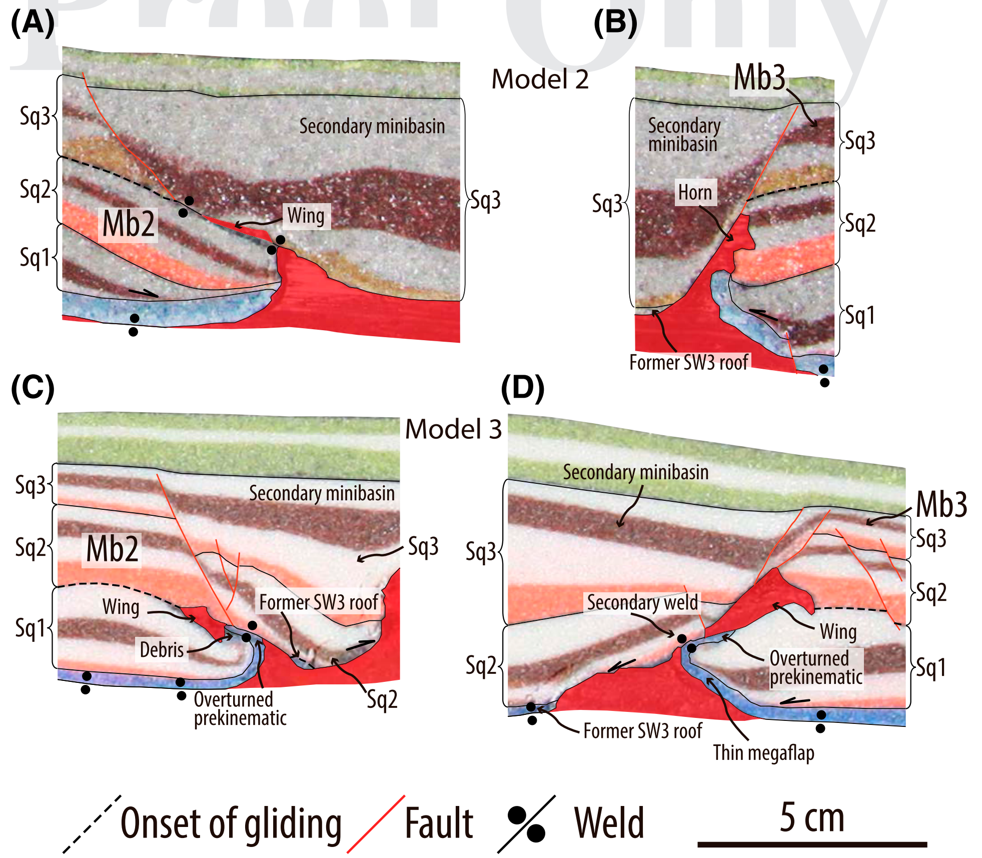

Figure 8. Detailed view and interpretation of the relationships between the primary and secondary minibasins, and tertiary welds around the collapsed salt wall 3 (SW3) in models 2 (A, B) and 3 (C, D). Further explanations in the text. Mb2 and Mb3 = minibasins 2 and 3; Sq1–Sq3 = synkinematic sequences 1–3.

to layers (sensu Rowan and Weimer, 1998). Q:29 Synkinematic sequence 3 shows a tapered geometry. However, the observed basinward thickening of synkinematic sequence 3 most likely responds to regional tilting rather than local downbuilding. Therefore, its geometry is interpreted as that of a layer sequence (Figure 5A). In model 4 (Figure 5D), the Mb1-equivalent raft consists of the prekinematic layer with a broadly conformable synkinematic sequence 1 deposited on top, with only minor lapping on both ends; synkinematic sequence 2 expands laterally over time (i.e., increases in line length). Both synkinematic sequences constitute layers. However, Mb1s in models 2 and 3 are markedly different, with both forming turtle structures (Figure 5B, C). In model 2, synkinematic sequences 1 and 2 were deposited under Q:30 downbuilding and conform to throughs and layers, respectively. Synkinematic sequence 2 laps onto and eventually is unconformable on both tips of the prekinematic layer. It also expands laterally further than synkinematic sequence 1 and is characterized by a thinning-upward infill. Synkinematic sequence 3 is formed by wedges that thicken and expand basinward, juxtaposed onto model salt. The model salt is eventually extruded on the model surface. Fully overturned sand packages are recognizable below the extruded model salt. Finally, the allochthonous salt is capped by the last layers of synkinematic sequence 3 (Figure 5B).

In model 3, Mb1 displays a narrower core fully welded at its base, with troughs belonging to the synkinematic sequence 1. The prekinematic layer becomes steeper toward flanking SW1 and SW2, onto which layers of the synkinematic sequence 2 lap and overlap, showing an outward depocenter expansion and shift (i.e., a turtle structure). Outward, the prekinematic layer reattains a shallower dip, onto which the layers of the synkinematic sequence 2 become thinner and condensed to be finally deposited onto the model salt. Layers of synkinematic sequence 3 also expand laterally onto model salt, constituting long diapir shoulders (Figures 5C, 6C). Once again, the tapered geometry of synkinematic sequences results from regional tilting; then, such sequence corresponds to a layer geometry.

The geometry of SW2 varies between models (Figures 4, 6, and 7). It appears as a vertical salt wall with a wide pedestal in model 1 (Figure 4A), whereas it presents a mushroom-like shape in model 2 (Figures 4B, 6B). In model 3, SW2 varies along strike from a wide salt wall topped by a condensed synkinematic sequence on a perched roof (Figure 4C) to an asymmetric salt wall with irregular shape depicting a diapir shoulder in its landward flank (Figure 6C). Such lateral changes are also observed in model 4, in which SW2 shows upward-narrowing geometries (Figure 4D) that laterally grade into smaller diapirs featuring salt wings (Figure 6D).

Q:31 Remarkable differences are also present for Mb2, Mb3, and the distal basin depocenter in between models 1 and 4 (Figure 7). In model 1, flanks of SW3 corresponding to Mb2 and the distal basin depocenter are broadly symmetrical (Figure 7A), showing a folded prekinematic layer, and synkinematic sequences 1, 2, and 3 conforming to troughs first and then layers, respectively (Figure 7A). Models 2–4 show a notable difference from model 1 as indicated by the collapse of the intervening salt wall between Mb2 and Mb3 (i.e., SW3) and the development of a raft system (Figure 4). Such collapse developed as a secondary minibasin (sensu Pilcher et al., 2011) for models 2 and 3, and as an expulsion rollover for model 4. Models 2 and 3 show well-developed turtle structures for Mb2 and Mb3, characterized by troughs (synkinematic sequence 1), followed by layers (synkinematic sequence 2) and wedges/troughs constituting the secondary minibasins. The secondary minibasins developed at different times in models 2 and 3, but in both cases they are associated with the onset of the dominant gliding in the system (i.e., between synkinematic sequence 2 and 3 in model 2, and between sequences 1 and 2 in model 3).

In models 2 and 3, Mb2 and Mb3 are turtle anticlines. They show a thicker core consisting of troughs with a central depocenter, whereas younger depocenters expand outward. Crestal collapse faults developed on their central positions. The infill of the collapsed SW3 is also different for both models 2 and 3. The secondary minibasin in model 2 displays a broad trough-like depocenter on its central position, which is bound by inward-dipping extensional faults soled into wings of allochthonous salt. A small triangular diapir is also present sideways to the central position of the secondary minibasin, indicative of stretching. However, the collapsed SW3 in model 3 shows sediment wedges that thicken into the collapsed salt wall belonging to the synkinematic sequence 2 (i.e., synchronous to **Q:32** dominant gliding onset). These wedges are overlaid by troughs of synkinematic sequence 3 that roof the collapsed salt wall. The edges of the secondary minibasins in models 2 and 3 are constituted by extensional faults linked downdip to collapsed salt wings (Figure 7B, C). These faults are listric and low angle or steeply dipping and planar whether they nucleate into bed-parallel salt wings or relic subvertical salt horns, respectively (Figure 8A, B). Model 3 displays megaflaps welded to minibasin boundaries. Salt wing remnants are preserved between these welds (Figure 8C, D). Another difference between the secondary minibasins of models 2 and 3 is the geometry of the remnant salt wall (compare Figure 7B, C). In model 2 (Figure 7B), a triangular-shaped diapir is present, whereas in model 3 (Figure 7C), the remnant salt wall is characterized by hooks, cusp-like features, and salt wings.

The shelf break to the distal section of model 4 is **Q:33** characterized by rafts and a collapsed salt wall that features an expulsion rollover (Figure 7D). The onset of model salt extrusion took place relatively early, at the beginning of sedimentation of synkinematic sequence 1. The most distal raft was covered by allochthonous model salt, onto which synkinematic sequence 2 was deposited and eventually tertiary welded. The internal geometry of the expulsion rollover conforms to sigmoids, with a centrally located depocenter that thins landward and basinward (Figure 7D).

To summarize, in our models, downbuilding is shown by vertically stacked synkinematic depocenters, thinning and lapping outward (i.e., troughs) on a prekinematic layer of even thickness. Erosional truncations either of megaflaps against synkinematic stratigraphy or between synkinematic strata are diagnostic of downbuilding. Conversely, the lateral truncation of the prekinematic stratigraphy against salt is diagnostic of salt-detached extension produced during dominant gliding. The transition from downbuilding to gliding is marked by a change in the internal architecture of minibasins shown by the truncation of the prekinematic stratigraphy by synkinematic strata and the lateral expansion of minibasins with time, as demonstrated by an increase in the line length of younger stratigraphic units, beside the collapse of minibasin-flanking salt walls. Q:34

DISCUSSION

Dominant Gliding versus Downbuilding Influence on Salt–Sediment Systems

Salt tectonics on rifted continental margins results from the combination of gravitational collapse, differential sedimentary loading, salt-detached extension, and salt evacuation (e.g., Brun and Fort, 2011, 2012; Rowan et al., 2012; Peel, 2014; Granado et al., 2016; Pichel and Jackson, 2020; Roca et al., 2021); those can be superimposed on crustal extension and regional thermal subsidence (e.g., Moragas et al., 2018; Granado et al., 2019; Strauss et al., 2021a, b; Epin et al., 2021). By means of analogue modeling, we investigated the controls of the prevailing mechanisms—either dominant gliding or downbuilding—on the evolution of salt–sediment systems and their record on the stratigraphic architecture of minibasins and structural styles. The challenge is to unravel the components of each mechanism (gliding versus downbuilding) when they are occurring simultaneously. In this sense, major differences in minibasin tectonostratigraphic architectures, diapir geometries, structural styles, welds, and sediment accommodation space through space and time have been found in our analogue models. All of these features are well illustrated by the end member models 1 and 4, whereas the intermediate spectrum is represented by models 2 and 3 (Figure 4).

One of the most striking results of the presented modeling is the difference in sediment accommodation space. By dominant gliding alone, model 4 accommodated two synkinematic sequences before complete basal welding and halting of downslope gliding after 72 hr. By means of pure downbuilding, model 1 accumulated three synkinematic sequences in less than half that time (Figure 2D). Sedimentation accumulation rates also varied through time in relation to the main driving mechanism, as well as across the modeled rifted margin (i.e., proximal basin, isolated-minibasin province, and distal basin and raft system). For the minibasin province, continuous linear trends of sedimentation rates represent dominant gliding, whereas sedimentation rates of pure downbuilding systems were characterized by an early linear trend followed by an exponential trend after 26 hr. After an initial phase of slow sinking and limited salt evacuation, pure downbuilding was found to be a very efficient mechanism for sediment trapping by salt evacuation. The efficiency of downbuilding in trapping sediments has already been suggested by the previous analogue modeling of Santolaria et al. (2021) and by subsidence analysis in real-world case studies (e.g., Strauss et al., 2021a, b). Widening of salt walls by cryptic extension accompanied by synkinematic sedimentation and the associated differential loading in secondary minibasins is also an efficient mechanism for sediment trapping, as observed in models 2 and 3. Secondary minibasins can attain thicknesses similar to those of the primary minibasins, and contrary to their original definition (Pilcher et al., 2011; Jackson and Hudec, 2017), can sink into the salt feeders of diapirs (i.e., autochthonous salt) and have the oldest postsalt stratigraphy (i.e., diapir roofs remnants) at their bases (model 3; Figures 4C; 7C; 8C, D).

In models with dominant gliding (i.e., models 2–4), extension was significantly focused seaward of the shelf break (Figures 3, 4). In models 2 and 3, minibasins on the shelf area display a progressive increase in the line length for younger synkinematic sequences in comparison with the older synkinematic. This line length increase seen through time can be readily observed by the presence of diapir shoulders. Most of the salt-detached extension took place seaward of the shelf break, as shown by the progressive widening and eventual collapse of SW3 (Figures 4, 6, 7) and the positive correlation in the number of rafts relative to the amount of dominant gliding (i.e., increasing from model 2 to 4; Figure 4). The most reasonable control for these changes in minibasin geometries and on the amount of extension through space and time is the change in the gradient of topography and sediment loading at the shelf break (Figure 4), as indicated in many natural systems (e.g., Brun and Fort, 2004, 2011, 2012; Rowan et al., 2004; Granado et al., 2016) and previous analogue modeling works (e.g., Ge et al., 1997; Gemmer et al., 2004; Adam and Krezsek, 2012). Q:35

As illustrated in our modeling results, the internal architecture of the minibasins and the profiles of flanking diapirs reflect the local pattern of salt flow and the regional dynamics of the modeled margin imposed by tilting and dominant gliding. Accordingly, the onset of gliding led to different responses of the modeled salt–sediment system. In the proximal basins, which are located within the proximal parts of the margin, the stratigraphic architecture that marks the onset of gliding is systematically consistent with wedges (Figures 4D, 5D). In those minibasins flanked by salt walls on either side (i.e., Mb1 and Mb2), layers (models 3 and 4) or wedges (model 2) form after the onset of gliding. In model 2, gliding led to minibasin tilting (Mb1) and the formation of a turtle (Mb2). Accommodation space is then filled by wedges thickening toward SW2 (Figures 5B, 7B). Conversely, gliding in model 3 results in the expansion of Mb1 at the expense of Mb2, whose flanks retreat, resulting in an asymmetric SW2 (Figures 6C, 9). Such minibasin architecture points to a preferential basinward flow of the evacuated model salt. In model 4, gliding promoted rapid basinward evacuation of model salt.

Timing of the onset of dominant gliding with respect to downbuilding is crucial regarding the structural geometries and stratigraphic architectures of minibasins (Figure 9). Diagnostic features that mark a change in the dominant mechanism (i.e., from pure downbuilding to dominant gliding) are the presence of diapir shoulders and perched roofs when gliding occurs before effective diapir roof piercement, or the collapse of minibasin flanks and deposition of wedges after effective diapir piercement (Figure 9). The presence of diapir shoulders thus is diagnostic of salt wall widening due to salt-detached extension and collapse. Early dominant gliding after downbuilding favors the formation of asymmetric salt walls (Figure 9A), whereas late dominant gliding after downbuilding favors more symmetric salt walls (Figure 9B). Since shoulders and perched roofs are formed upon early gliding (model 3), secondary minibasins that develop after the collapse of salt walls can have the oldest postsalt stratigraphy at their bases (Figures 7C; 10A, B). Such a feature has not been observed when gliding occurs later after downbuilding (model 2; Figure 7B).

General concepts and diagnostic features can be gained from the results of our work as to the interplay of downbuilding and gliding on salt-bearing rifted margins (Figure 10). Downbuilding is represented by vertically stacked synkinematic depocenters on top of a prekinematic layer, along with the erosional truncation of upturned megaflaps and early synkinematic strata and the presence of resedimented salt debris and prekinematic strata in the downbuilt stratigraphy. A component of concomitant extension and the inception of gliding is shown by the sharp truncation of sedimentary sequences against the salt and the formation of diapir shoulders or perched flaps (Figure 10A). The presence of shoulders and flaps is diagnostic of salt wall widening due to salt-detached extension before salt wall collapse; hence, diapir shoulders mark a change in the dominant mechanism (i.e., from pure downbuilding to dominant gliding). However, gliding following downbuilding is

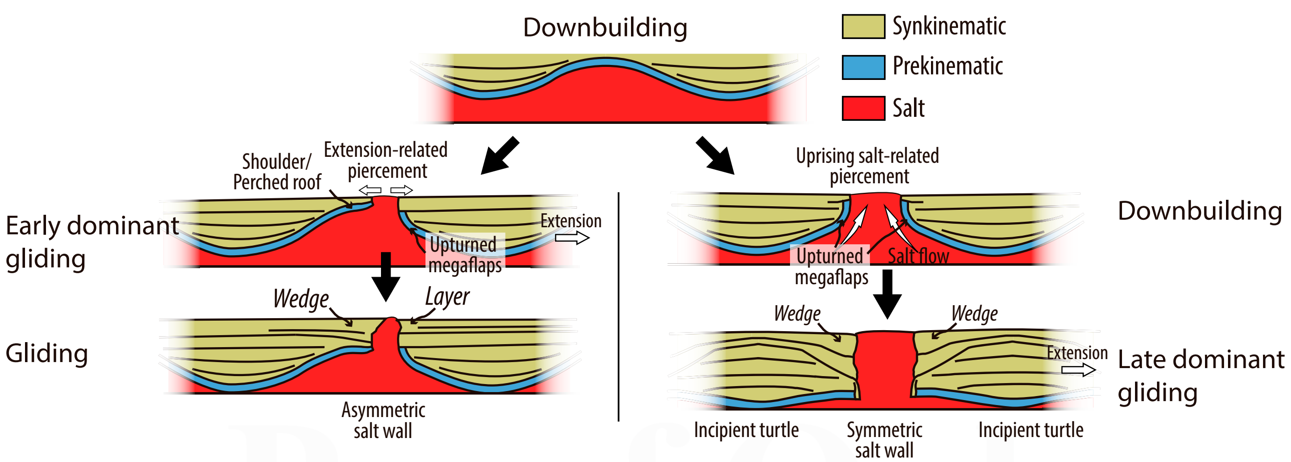

Figure 9. Diagnostic geometries of downbuilding and dominant gliding when the onset of gliding occurs early (left column, model 3) or late (right column, model 2) with respect to downbuilding.

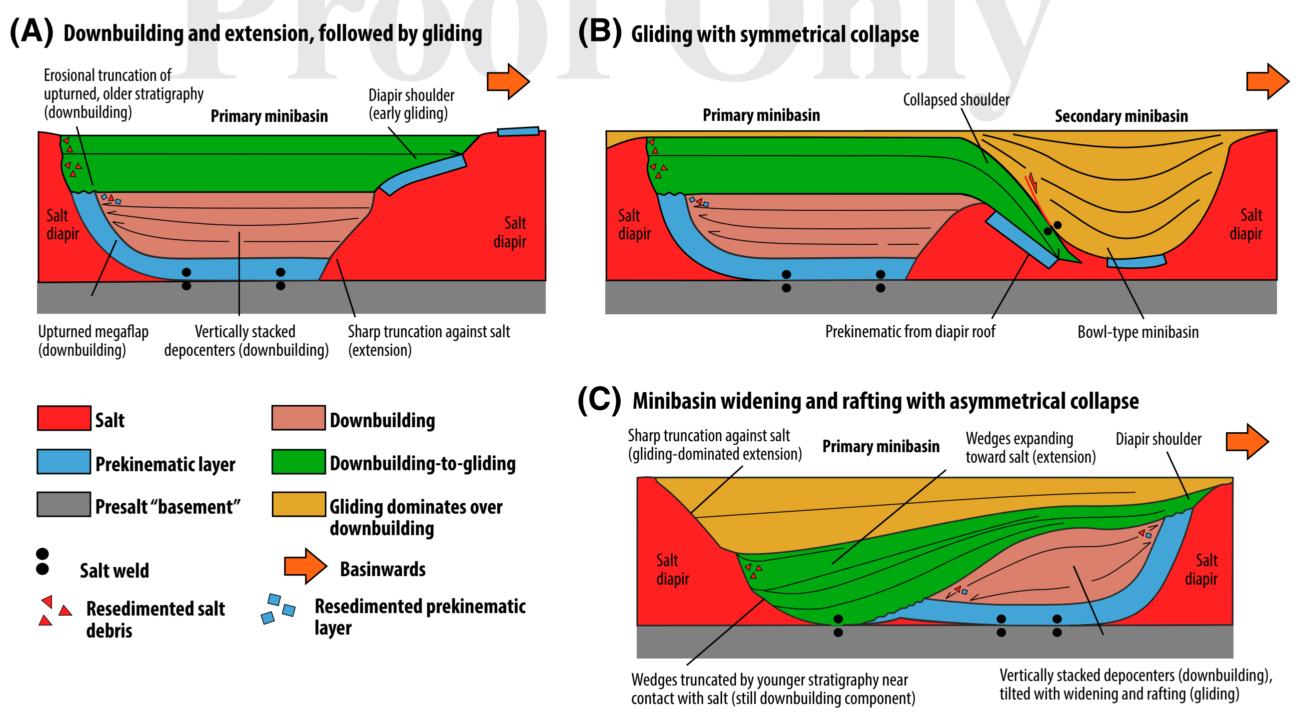

Figure 10. Key diagnostic features illustrating the interplay of downbuilding and dominant gliding. (A) Downbuilding and extension, followed by gliding. (B) Gliding with symmetrical collapse. (C) Minibasin widening and rafting with asymmetrical collapse.

indicated by the collapse of diapir shoulders and the formation of symmetrical (bowl type) secondary minibasins (Figure 10B). Minibasin widening and rafting occur when gliding dominates over downbuilding (Figure 10C). In these settings, gliding and salt-detached extension are shown by the development of large sedimentary wedges expanding toward the salt. However, wedges truncated by younger stratigraphy near the contact with salt can indicate the occurrence of a coeval downbuilding component; resediment salt debris close to the salt–sediment contact would additionally support the downbuilding component. As the importance of downbuilding diminishes in favor of gliding, wedges expand toward the salt, and the salt–sediment contact is represented by a sharp truncation of sediments against salt.

Additional key observations for the presented analogue models are the distribution, geometry, and kinematics of welds. Welds are of significant importance in petroleum systems analysis (e.g., Rowan, 2004b; Wagner, 2011), since understanding their geometry and kinematics are important in assessing the timing of hydrocarbon migration from presalt to postsalt units. Understanding of welds is also important for geological storage considerations (e.g., Roelofse et al., 2019). Minibasins developed by pure downbuilding (i.e., model 1) show primary welds in their central position (i.e., linear features in 3-D). However, upon dominant gliding (i.e., model 4) welds that extend along the whole base of the prekinematic layer of rafted blocks (Figure 4A, D). When down- Q:36 building was followed by dominant gliding (models 2 and 3), primary welds evolved from being located in the central parts of minibasins (i.e., pure downbuilding) to lengthening with the collapse of salt walls (Figures 3B, C; 4B, V; 10). Secondary welds are less Q:37 common in our models (Figures 4C, 8D). Nevertheless, they also developed upon the coalescence of distal rafts in model 3 (Figure 4). Secondary welds developed at the margins of secondary minibasins, on top of overturned megaflaps involving the prekinematic layers and upturned strata of synkinematic sequence 1 (Figures 7C, 8D). Tertiary welds devel- Q:38 oped on top of distal rafts (Figure 7D) and developed associated with an expulsion rollover formed after the collapsed salt wall at the shelf break (model 4; Figures 4D, 7D). Our models have shown that dom- Q:39 inant gliding produces larger welding areas at the base of minibasins early on (i.e., model 4), whereas pure downbuilding favors comparatively smaller welding areas (i.e., model 1). As minibasins glide and salt walls collapse, the areas of welding can increase through time, as shown in models 2 and 3.

Secondary minibasins can also weld to adjacent primary minibasins (Figure 10B). When secondary minibasins sink into and evacuate allochthonous salt, subhorizontal tertiary welds juxtapose subhorizontal layers on top of primary minibasins with subhorizontal or tilted strata. If secondary minibasins sink into the feeders of former salt walls, then they weld to the sides of primary minibasins (Figure 10B) and to the base of the autochthonous salt, thus forming the so-defined bowl and bucket welds, respectively (i.e., Pilcher et al., 2011). In our models 2 and 3, such welds develop after the evacuation of salt from subhorizontal salt wings (Figure 8A), but they can also form after subvertical salt horns (Figure 8B). In our models, these welds were also reactivated as extensional faults (Figures 7B, C; 8A, C, D; 10B).

Comparison with Natural Examples

Offshore South Gabon

During the Late Jurassic, continental rifting began between South America and Africa and led to the opening of the South Atlantic realm (see Dupré et al., 2007, and references therein). Crustal separation and onset of oceanic spreading took place ca. 133 Ma (i.e., according to magnetic anomaly M11) in the Cape Basin of South Africa and propagated northward to the Gulf of Guinea. Complete separation between South American and African continents occurred in the late Albian–Cenomanian with the opening of the equatorial Atlantic Ocean. The South Atlantic salt basin of western Africa is bound by the volcanic Walvis Ridge to the south and the Cameroon volcanic trend to the north (see Kukla et al., 2018, for a review). The region between (i.e., from Angola to the south to Cameroon to the north) is characterized by mobile postrift Aptian evaporites. In the South Gabon margin (Figure 11), carbonate and siliciclastic units were deposited onto the Aptian evaporites and include the Albian lower Madiela carbonate prerafting section, the Albian midupper Madiela, and the Cenomanian–Maastrichtian Cap Lopez and overlying units, which are represented by a mixed carbonate-siliciclastic stratigraphy associated with rafting and salt evacuation (Figure 11A). The Cenozoic is represented by a siliciclastic system of shales and coarse-grained clastics, which show a waning but still synkinematic (i.e., synrafting) nature.

In more detail, the lower Madiela carbonate section constitutes the core of rafts and shows depocenters that are clearly vertically stacked and constitute rather symmetric structures originally flanked by linear salt walls (Figure 11A). In contrast, the midupper Madiela section is characterized by large wedges that expand onto the Aptian salt and form largely asymmetric structures developed after the collapse of the salt walls that formed earlier (e.g., Moore and Blanchard, 2017).

The line length measurements for a dip section shown in Figure 11A show a progressive line length increase with time (i.e., red line [top of lower Madiela Formation] versus purple line [top of Cap Lopez Formation]), which is a clear indication for thin-skinned extension and rafting above the Albian salt (i.e., minibasin widening). Model 3 displays geometries similar to those in the South Gabon dip section (see Figure 11B), including the vertically stacked depocenters in the core of the minibasins and the subsequent development of outward expanding wedges into the collapsing salt walls (i.e., which result in cryptic extension related to rafting). Those wedges sometimes become suddenly thinner toward the adjacent inflated salt, thus being indicators of a certain component of downbuilding in addition to thin-skinned extension. This downbuilding component is also revealed by a shorter restored line length of the initial synkinematic layer in comparison with that of the prekinematic (Figure 11B), being then followed by progressively increasing line lengths that testify to the dominance of gliding.

On the map view, raft structures have an elongated pattern that varies in orientation across the South Gabon margin (e.g., Moore and Blanchard, 2017). Such a pattern of rafting has also been shown for other salt basins, such as those in Angola (e.g., Ge et al., 2020) or the Congo Basin (Anderson et al., 2000; Rouby et al., 2002). Likewise, our experiments that include dominant gliding (i.e., models 2–4) show such elongated patterns and the variable orientations of distal rafts beyond the shelf break, which are mostly associated with rotations around the vertical axes (Figure 3).

To summarize, our models comprising an initial phase of pure downbuilding followed by dominant gliding show strong similarities to natural examples

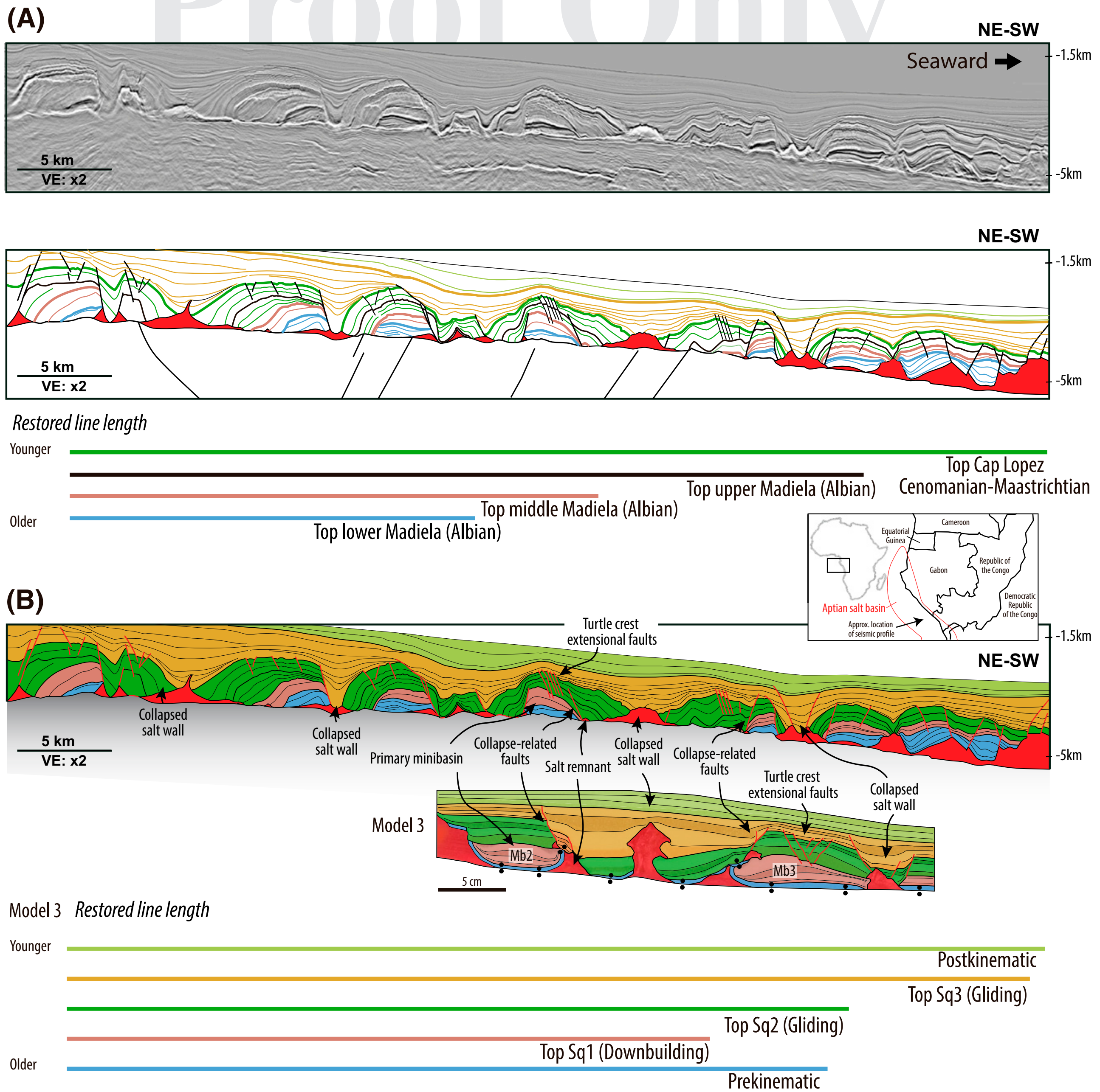

Figure 11. (A) Dip line from a depth-migrated three-dimensional survey from offshore Gabon and line drawing carried by the authors (modified from Moore and Blanchard, 2017). Note the line-length increase over time (red, green, blue, and purple horizons), which demonstrates salt-detached rafting. The internal geometries of lower Madiela carbonates (red horizons) in the core of turtle anticlines and rafts are indicative of early salt evacuation by downbuilding. (B) Colored line drawing. Colors have been chosen for the sake of comparison to our analogue models. Mb2 and Mb3 = minibasins 2 and 3; Sq1–Sq3 = synkinematic sequences 1–3; VE = XX.

Q:60

of rifted margins with salt tectonics, as exemplified by the South Gabon Basin (Figure 11). Therefore, it can be postulated that the inception of salt tectonics in this basin seems to have been controlled by early extension, as indicated by the sharp truncation of lower Madiela reflectors against the Aptian salt, but being suddenly affected by differential loading and downbuilding by carbonate growth, as indicated by the internal vertical stacking of the lower Madiela carbonates, and their truncations against younger and unconformable midupper Madiela series. Early loading by carbonate aggradation triggered salt evacuation and the formation of a series of dominantly linear diapirs (i.e., salt walls) at the margins of the shallow water platforms. Similar relationships have been identified for Triassic minibasins in the Northern Calcareous Alps of Austria (Granado et al., 2019). Truncations of an Anisian prekinematic layer against Permian salt on one minibasin side, as well as the erosional truncation of the same upturned layer by younger Triassic synkinematic units on the other minibasin side, have been defined by field mapping and balanced cross section construction (Strauss et al., 2021b, their figure 3). Salt-detached extension along the Permian salt allowed for the inception of rafting, fostering salt evacuation by downbuilding produced by carbonate aggradation.

Gravity-Driven Salt Tectonics in the Cotiella Thrust Sheet (Southern Pyrenees)

The Cotiella Massif in the southern Pyrenees constitutes a seismic-scale example of a salt-detached postrift extensional basin developed on the Bay of Biscay-Pyrenean rifted margin (McClay et al., 2004). The Cotiella salt-detached system developed via the Late Cretaceous gravity-driven collapse of a carbonate platform above Upper Triassic salt. The internal structure of Cotiella is currently represented by up to four middle Coniacian to early Santonian subbasins (namely Cotiella, Armeña, Peña de Mediodía, and Seira; see López-Mir et al., 2014, 2015), characterized by growth geometries (Figure 12A). These subbasins involve shallow water marine limestones and sandstones interfingering with pelagic carbonates (Souquet, 1967; Garrido-Megías and Ríos-Aragües, 1972; Séguret, 1972). Cumulatively, these units constitute as much as 6 km of synkinematic growth strata deposited on the postrift, thermally subsiding continental margin (McClay et al., 2004; López-Mir et al., 2014, 2015). The observed rollovers in some subbasins account for extensional collapse. However, the internal geometry of the basins and the detailed structure of sediments near the salt contact, facies distribution, and evidence of Triassic salt-derived detritus (i.e., quartz bipyramidal crystals) demonstrate that some of the Cotiella subbasins were initially minibasins surrounded by salt walls. These salt walls were subsequently squeezed during the Pyrenean contractional deformation (López-Mir et al., 2014). The extensional faults are only partially inverted despite the transport of the Pyrenean thrust sheets tens of kilometers southward (Muñoz et al., 2018). Former flanking diapirs have been squeezed and are currently recognizable as secondary welds. The prekinematic layer of these salt-detached minibasins is represented by Cenomanian shallow-water carbonates, directly juxtaposed to the Triassic salt, and being locally overturned as a result of Pyrenean shortening. The large stratigraphic omission of prerift and synrift units (i.e., ~110 m.y., from Jurassic to Albian) has been interpreted as resulting from either large erosion on the rifted margin shoulder, and/or nondeposition due to the presence of a large salt plateau (McClay et al., 2004; López-Mir et al., 2014, 2015).

An immediate question while interpreting the structure and the stratigraphic record of the Cotiella minibasins concerns the mechanisms that have formed the accommodation space for up to 6-km-thick sedimentary successions in a short time span (~3 m.y.); in other words, what is the contribution of dominant gliding versus downbuilding during the evolution of these basins? In this respect, the infill of the Cotiella minibasins mainly displays a fanning geometry, with successions expanding landward. However, each of the minibasins shown in Figure 12 possesses slight differences in internal architecture (Figure 12A, B). The southernmost Cotiella minibasin is the thickest and largest basin showing a fanning geometry of subhorizontal to overturned growth strata. This geometry matches that found on listric faults, where stratigraphic sequences thicken toward and up to the fault plane. According to our analogue modeling results, truncation of the lower synkinematic unit underneath the intermediate indicates a dominant downbuilding mechanism (Figure 12B). This interpretation is consistent with the presence of salt-sourced detritus in the lower unit during the development of the salt wall between the Cotiella and Armeña subbasins. Nevertheless, the truncation of the prekinematic succession against the salt is consistent with extensional deformation at the onset of synkinematic sedimentation. The upper two synkinematic units developed via a dominant gliding mechanism, as demonstrated by their wedge geometry. Conversely, the northernmost preserved Mediodía minibasin shows moderate wedging, and its internal structure mainly consists of subparallel to moderately southward expanding sedimentary packages. The prekinematic succession shows a basinward tilting once the Pyrenean contractional deformation is restored, thus suggesting a dominant

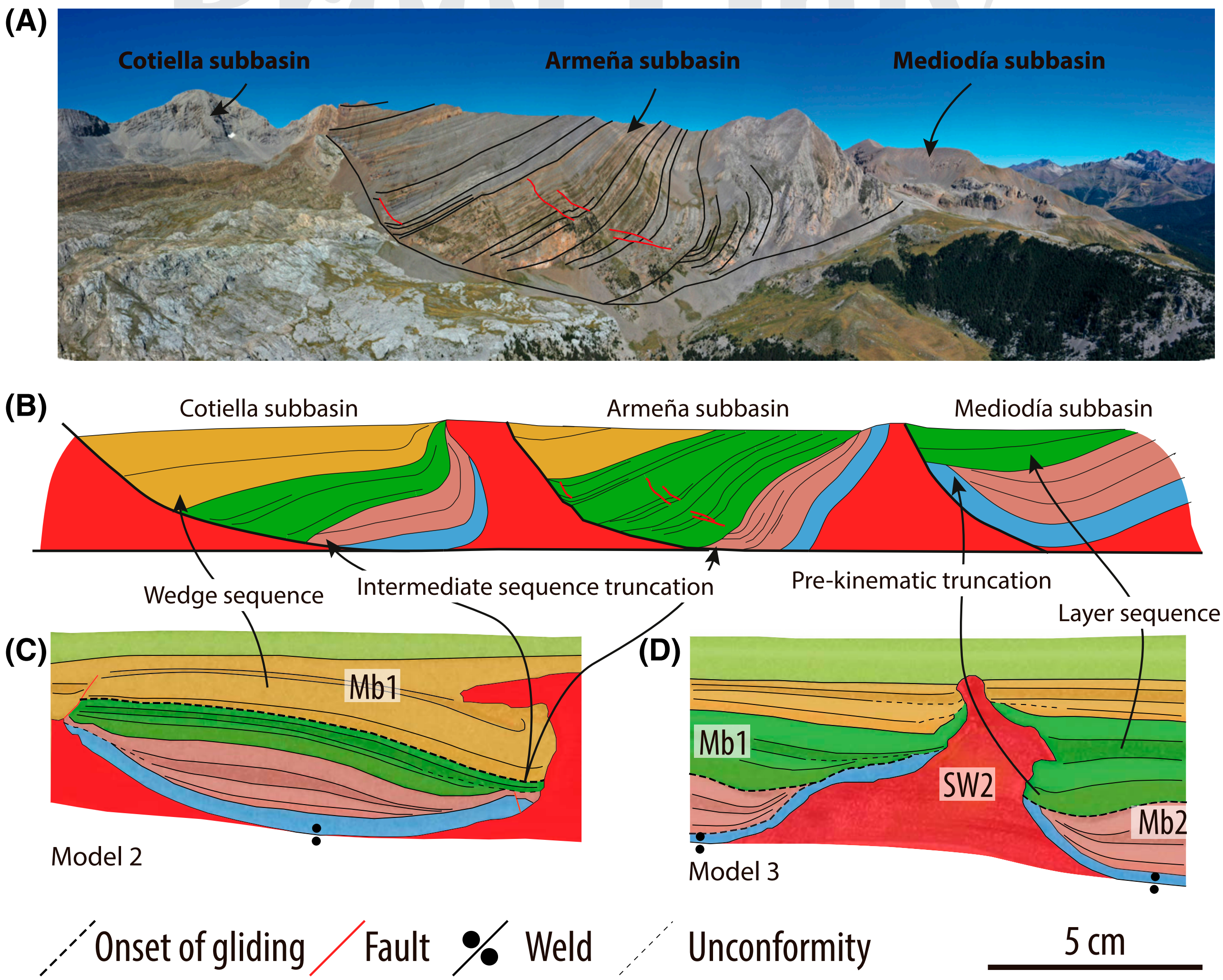

Q:61

Figure 12. (A) Northwest-looking drone-acquired panorama of the southern Pyrenees Cotiella Massif, showing the three main salt-related subbasins of Cotiella, Armeña, and Mediodía. (B) Line drawing interpretation of the main structural geometries and tectonostratigraphic architectures, with the effects of contractional deformation and related erosion removed. These geometries and architectures include a prekinematic layer (blue), which is truncated against the Triassic salt and/or against younger unconformable synkinematic sequences; a first synkinematic package (brown) of uneven thickness, which laps onto the prekinematic and is truncated by unconformable overlying synkinematic sequences; and a synkinematic sequence (green), which expands toward the Triassic salt and is also locally truncated by the overlying synkinematic sequence. Colors have been chosen for the sake of comparison to our analogue models. (C) Close-up of model 2. (D) Close-up of model 3. Mb1 and Mb2 = minibasins 1 and 2; SW2 = salt wall 2.

downbuilding mechanism during the early stages of synkinematic sedimentation (Figure 12B). The Armeña minibasin (Figure 12B) represents a hybrid scenario between the Cotiella and Mediodía subbasins. Basin infill architecture shows a wedge geometry that suggests a dominant gliding mechanism during sedimentation. However, the syncline geometry with basinward shifted depocenters and the structure of the sediment–salt interface attest to a downbuilding mechanism. The overall architecture of the Armeña minibasin has been interpreted as a combination of listric faulting together with salt evacuation toward the footwall (i.e., slightly sigmoidal features). Similar geometries have been defined for counterregional salt–sediment systems such as expulsion rollovers. However, we want to comment on the importance of geometries and basin architectures as diagnostic criteria of combined sedimentary and salt tectonics processes. We believe that this combination of processes is well represented in our analogue models, as, for example, in the Mb1 and Mb2 of models 2 and 3 (Figure 12C, D), the wedge sequences on the secondary minibasins

(Figure 7C), and the expulsion rollover in model 4 (Figure 7C). The tectono-stratigraphic architecture and angular relationships found in our analogue models provide valuable constraints to interpret the structure of the Cotiella minibasins but also to reconstruct those areas above the present-day erosional level.

CONCLUSIONS

Our modeling program was focused on simulating a thermally subsiding rifted margin with a confined, fault-bound late synrift to early postrift salt basin. End member models included pure downbuilding on the one hand and dominant gliding on the other hand. The spectrum between those was completed by modeling different amounts of downbuilding versus dominant gliding. Our results provide key diagnostic structural geometries and tectono-stratigraphic architectures between minibasins driven by downbuilding and dominant gliding on salt-bearing rifted margin settings. Special emphasis has been placed on deciphering the record of simultaneous downbuilding and gliding and that when gliding dominates over downbuilding.

In the very early stages, dominant gliding is seen as an efficient process for sediment accommodation space creation. However, once downbuilding evolves from an early linear trend to an exponential trend of sediment accumulation with time, downbuilding becomes a more efficient mechanism to trap sediments. The diagnostic features of salt-detached extension are shown by sharp truncations of strata against salt and the expansion of sediment wedges toward inflated salt. If extension following downbuilding predates the piercement of the overburden (i.e., short phase of downbuilding), then diapir shoulders develop. The presence of diapir shoulders is diagnostic of salt wall widening due to salt-detached extension previous to salt wall collapse; hence, diapir shoulders mark a change in the dominant mechanism (i.e., from pure downbuilding to dominant gliding). When pure downbuilding is the main mechanism responsible for minibasin formation or when downbuilding lasts for a longer period of time than extension, the formation of diapir shoulders is precluded. The presence of upturned to overturned prekinematic layers truncated younger unconformable sequences, as well as the presence of synkinematic debris derived from the salt and the oldest postsalt stratigraphy, are clear indicators of differential sedimentary loading and downbuilding. When gliding dominates over downbuilding, previous salt walls collapse, leading to the formation of turtle structures, secondary minibasins, and large wedges. When shoulders and perched roofs develop, the bases of secondary minibasins can be constituted by the oldest postsalt stratigraphy overlaid by condensed sedimentary sequences. Salt-detached extension is shown by an increase in the line length of stratigraphic units with time. The occurrence of downbuilding before gliding can be observed by shorter line lengths in the early synkinematic units, followed by a sudden line length increase with the presence of diapir roofs, the formation of secondary minibasins by salt wall collapse, and the inception of rafting. Based on our results, downbuilding represents most likely a prebreakup process (i.e., thinning phase after stretching) before extension is focused in the shelf and in the necking area, where hyperextension forms a regional slope enhanced by thermal subsidence, fostering dominant gliding over downbuilding.

REFERENCES CITED

Adam, J., J. Urai, B. Wieneke, O. Oncken, K. Pfeiffer, N. Kukowski, J. Lohrmann, S. Hoth, W. van der Zee, and J. Schmatz, 2005, Shear localisation and strain distribution during tectonic faulting - new insights from granular flow experiments and high-resolution optical image correlation techniques: Journal of Structural Geology, v. 27, no. 2, p. 283–301, doi:10.1016/j.jsg.2004.08.008.

Anderson, J. E., J. Cartwright, S. J. Drysdall, and N. Vivian, 2000, Controls on turbidite sand deposition during gravity-driven extension of a passive margin: Examples from Miocene sediments in block 4, Angola: Marine and Petroleum Geology, v. 17, no. 10, p. 1165–1203, doi:10.1016/S0264-8172(00)00059-3.

Brun, J.-P., and X. Fort, 2004, Compressional salt tectonics (Angolan margin): Tectonophysics, v. 382, no. 3–4, p. 129–150, doi:10.1016/j.tecto.2003.11.014.

Brun, J.-P., and X. Fort, 2011, Salt tectonics at passive margins: Geology versus models: Marine and Petroleum Geology, v. 28, no. 6, p. 1123–1145, doi:10.1016/j.marpetgeo.2011.03.004.

Brun, J.-P., and X. Fort, 2012, Salt tectonics at passive margins: Geology versus models - Reply: Marine and Petroleum Geology, v. 37, no. 1, p. 195–208, doi:10.1016/j.marpetgeo.2012.04.008.

Brun, J.-P., and T. P.-O. Mauduit, 2008, Origin of rollovers in salt tectonics: The inadequacy of the listic fault

Proof Only

model: Tectonophysics, v. 457, 11 p., doi:11.1116/j.tecto.2007.11.038. Q:41

Callot, J.-P., J.-F. Salel, J. Letouzey, J.-M. Daniel, and J.-C. Ringenbach, 2016, Three-dimensional evolution of salt-controlled minibasins: Interactions, folding, and megaflap development: AAPG Bulletin, v. 100, no. 9, p. 1419–1442, doi:10.1306/03101614087.

Chenin, P., G. Manatschal, J.-F. Ghienne, and P. Chao, 2021, The syn-rift tectono-stratigraphic record of rifted margins (part II): A new model to break through the proximal/distal interpretation frontier: Basin Research, v. 34, no. 2, p. 489–532, doi:11.1111/bre.12628.

Chenin, P., S. M. Schmalholz, G. Manatschal, and G. D. Karner, 2018, Necking of the lithosphere: A reappraisal of basic concepts with thermo-mechanical numerical modeling: Journal of Geophysical Research. Solid Earth, v. 123, no. 6, p. 5279–5299, doi:10.1029/2017JB014155.

Davison, I., J. Pindell, and J. Hull, eds., 2021, The basins, orogens and evolution of the southern Gulf of Mexico and northern Caribbean: Geological Society, London, Special Publications 2021, v. 504, p. 1–27, doi:10.1144/SP504-2020-218.

Davy, Ph., and P. R. Cobbold, 1991, Experiments on shortening of a 4-layer model of the continental lithosphere: Tectonophysics, v. 188, no. 1–2, p. 1–25, doi:10.1016/0040-1951(91)90311-F.

Dell’Ertole, D., and W. P. Schellart, 2013, The development of sheath folds in viscously stratified materials in simple shear conditions: An analogue approach: Journal of Structural Geology, v. 56, p. 129–141, doi:10.1016/j.jsg.2013.09.002.

Dupré, S., G. Bertotti, and S. Cloetingh, 2007, Tectonic history along the South Gabon Basin: Anomalous early post-rift subsidence: Marine and Petroleum Geology, v. 24, no. 3, p. 151–172, doi:10.1016/j.marpetgeo.2006.11.003.

Duval, B. C., C. Cramez, and M. P. A. Jackson, 1992, Raft tectonics in the Kwanza Basin, Angola: Marine and Petroleum Geology, v. 9, no. 4, p. 389–404, doi:10.1016/0264-8172(92)90050-O.

Epin, M. E., G. Manatschal, F. Sapin, and M. G. Rowan, 2021, The tectono-magmatic and subsidence evolution during lithospheric breakup in a salt-rich rifted margin: Insights from a 3D seismic survey from southern Gabon: Marine and Petroleum Geology, v. 128, 105005, XX p., doi:10.1016/j.marpetgeo.2021.105005. Q:42

Ferrer, O., O. Gratacós, E. Roca, and J. A. Muñoz, 2017, Modeling the interaction between presalt seamounts and gravitational failure in salt-bearing passive margins: The Messinian case in the northwestern Mediterranean Basin: Interpretation, v. 5, no. 1, p. SD99–SD117, doi:10.1190/INT-2016-0096.1.

Garrido-Megías, A., 1973, Estudio geológico y relación entre tectónica y sedimentación del Secundario y Terciario de la vertiente meridional pirenaica en su zona central (provincias de Huesca y Lérida), Ph.D. dissertation, University of Granada, Granada, Spain, XX p. Q:43

Garrido-Megías, A., and L. M. Ríos-Aragües, 1972, Síntesis geológica del secundario y terciario entre los ríos Cinca y Segre (Pirineo central de la vertiente sur-pirenaica, provincias de Huesca y Lérida): Boletín Geológico y Minero de España, v. 83, no. 0001, p. 1–47. Q:44

Ge, H., M. P. A. Jackson, and B. C. Vendeville, 1997, Kinematics and dynamics of salt tectonics driven by progradation: AAPG Bulletin, v. 81, no. 3, p. 398–423.

Ge, Z., R. L. Gawthorpe, A. Rotevatn, L. Zijerveld, C. A.-L. Jackson, and A. Oluboyo, 2020, Minibasin depocentre migration during diachronous salt welding, offshore Angola: Basin Research, v. 32, p. 875–893, doi:10.1111/bre.12404.

Ge, Z., M. Warsitzka, M. Rosenau, and R. L. Gawthorpe, 2019, Progressive tilting of salt-bearing continental margins controls thin-skinned deformation: Geology, v. 47, no. 12, p. 1122–1126, doi:10.1130/G46485.1.

Gemmer, L., S. J. Ings, S. Medeved, and C. Beaumont, 2004, Salt tectonics driven by differential sediment loading: Stability analysis and finite-element experiments: Basin Research, v. 16, no. 2, p. 199–218, doi:10.1111/j.1365-2117.2004.00229.x. Q:45

Goteti, R., S. J. Ings, and C. Beaumont, 2012, Development of salt minibasins under uneven sedimentation: Earth and Planetary Science Letters, v. 339–340, p. 113–116.

Graham, R., M. Jackson, R. Pilcher, and B. Kilsdonk, 2012, Allochthonous salt in the sub-Alpine fold-and-thrust belt of Haute Provence, France, *in* G. I. Alsop, S. G. Archer, A. J. Hartley, N. T. Grant, and R. Hodgkinson, eds., Salt tectonics, sediments and prospectivity: Geological Society, London, Special Publications 2012, v. 363, p. 595–615, doi:10.1144/SP363.30.

Granado, P., E. Roca, P. Strauss, K. Pelz, and J. A. Muñoz, 2019, Structural styles in fold-and-thrust belts involving early salt structures: The Northern Calcareous Alps (Austria): Geology, v. 47, no. 1, p. 51–54, doi:10.1130/G45281.1.

Granado, P., J. B. Ruh, P. Santolaria, P. Strauss, and J. A. Muñoz, 2021, Stretching and contraction of extensional basins with prerift salt: A numerical modeling approach: Frontiers in Earth Science (Lausanne), v. 9, 648937, 24 p., doi:10.3389/feart.2021.648937.

Granado, P., R. Urgeles, F. Sábat, E. Albert-Villanueva, E. Roca, J. A. Muñoz, N. Mazzucca, and R. Gambini, 2016, Geodynamical framework and hydrocarbon plays of a salt giant: The NW Mediterranean Basin: Petroleum Geoscience, v. 22, no. 4, p. 309–321, doi:10.1144/petgeo2015-084.

Hamblin, W. K., 1965, Origin of ‘reverse drag’ on the downthrow side of normal faults: Geological Society of America Bulletin, v. 76, no. 10, p. 1145–1164, doi:10.1130/0016-7606(1965)76[1145:OORDOT]2.0.CO;2.

Harrison, J. C., and M. P. A. Jackson, 2014, Exposed evaporite diapirs and minibasins above a canopy in central Sverdrup Basin, Axel Heiberg Island, Arctic Canada: Basin Research, v. 26, no. 4, p. 567–596, doi:10.1111/bre.12037.

Hudec, M. R., and M. P. A. Jackson, 2007, Terra infirma: Understanding salt tectonics: Earth-Science Reviews, v. 82, no. 1–2, 28 p., doi:10.1016/j.earscirev.2007.01.001.

Hudec, M. R., M. P. A. Jackson, and D. D. Schultz-Ela, 2009, The paradox of minibasin subsidence into salt: Clues to the evolution of crustal basins: Geological Society of America Bulletin, v. 121, p. 201–221, doi:10.1130/B26275.1. Q:46

Jackson, C. A.-L., O. B. Duffy, N. Fernandez, T. P. Dooley, M. R. Hudec, M. P. A. Jackson, and G. Burg, 2019, The stratigraphic record of minibasin subsidence, Precaspian Basin, Kazakhstan: Basin Research, v. 32, no. 4, p. 739–763, doi:10.1111/bre.12393.

Jackson, M. P. A., and C. Cramez, 1989, Seismic recognition of salt welds in salt tectonics regimes, *in* W. P. S. Ventress, D. G. Bebout, B. F. Perkins, and C. H. Moore, eds., Gulf of Mexico salt tectonics, associated processes and exploration potential: Tulsa, Oklahoma, SEPM Special Publication 10, p. 66–71, doi:10.5724/gcs.89.10.0066.

Jackson, M. P. A., and M. R. Hudec, 2017, Salt tectonics: Principles and practice: Cambridge, United Kingdom, Cambridge University Press, 498 p., doi:10.1017/9781139003988.

Jackson, M. P. A., and C. J. Talbot, 1991, A glossary of salt tectonics: Austin, Texas, The University of Texas at Austin, Bureau of Economic Geology Geological Circular 91, 44 p. Q:47

Koyi, H., M. K. Jenyon, and K. Petersen, 1993, The effect of basement faulting on diapirism: Journal of Petroleum Geology, v. 16, no. 3, p. 285–312, doi:10.1111/j.1747-5457.1993.tb00339.x.

Kukla, P. A., F. Strozyk, and W. U. Mohriak, 2018, South Atlantic salt basins – Witnesses of complex passive margin evolution: Gondwana Research, v. 53, p. 41–57, doi:10.1016/j.gr.2017.03.012.

Lehner, P., 1969, Salt tectonics and Pleistocene stratigraphy on continental slope of northern Gulf of Mexico: AAPG Bulletin, v. 53, p. 2431–2479.

Li, S., F. Strozyk, S. Abe, H. van Gent, P. Kukla, and J. L. Urai, 2012, A method to evaluate long-term rheology of Zechstein salt in the Tertiary, *in* P. Berest, M. Ghoreychi, F. Hadj-Hassen, and M. Tijani, eds., Mechanical behavior of salt VII: London, Taylor & Francis, p. 215–220, doi:10.1201/b12041-31. Q:48

Li, S., and J. L. Urai, 2016, Rheology of rock salt for salt tectonics modeling: Petroleum Science, v. 13, no. 4, p. 712–724, doi:10.1007/s12182-016-0121-6. Q:49

Lohrmann, J., N. Kukowski, J. Adam, and O. Oncken, 2003, The impact of analogue material properties on the geometry, kinematics and dynamics of convergent sand wedges: Journal of Structural Geology, v. 25, no. 10, p. 1691–1711, doi:10.1016/S0191-8141(03)00005-1.

López-Mir, B., J. A. Muñoz, and J. García-Senz, 2014, Restoration of basins driven by extension and salt tectonics: Example from the Cotiella Basin in the central Pyrenees: Journal of Structural Geology, v. 69, part A, p. 147–162, doi:10.1016/j.jsg.2014.09.022.

López-Mir, B., J. A. Muñoz, and J. García-Senz, 2015, Extensional salt tectonics in the partially inverted Cotiella post-rift basin: International Journal of Earth Sciences, v. 104, p. 419–434, doi:10.1007/s00531-014-1091-9.

Mancini, E. A., M. Badali, T. M. Puckett, J. C. Llinas, and W. C. Parcell, 2001, Mesozoic carbonate petroleum systems in the northeastern Gulf of Mexico area, *in* R. H. Fillon, N. C. Rosen, P. Weimer, A. Lowrie, H. Pettingill, R. L. Phair, H. H. Roberts, and H. H. van Hoom, eds., Petroleum systems of deep-water basins–Global and Gulf of Mexico experience: Tulsa, Oklahoma, SEPM Special Publication 21, p. 423–452, doi:10.5724/gcs.01.21.0423.

McClay, K. R., J. A. Muñoz, and J. García-Senz, 2004, Extensional salt tectonics in a contractional orogen: A newly identified tectonic event in the Spanish Pyrenees: Geology, v. 32, no. 9, p. 737–740, doi:10.1130/G20565.1.

Moore, V. M., and R. H. Blanchard, 2017, Raft-related structures of the Albian Madiela formation, offshore South Gabon: AAPG Search and Discovery article 51373, accessed XX, https://www.searchanddiscovery.com/documents/2017/51373moore/ndx_moore.pdf.

Moragas, M., J. Vergés, E. Saura, J.-D. Martín-Martín, G. Messager, Ó. Merino-Tomé, I. Suárez-Ruiz, et al., 2018, Jurassic rifting to postrift subsidence analysis in the Central High Atlas and its relation to salt diapirism: Basin Research, v. 30, p. 336–362, doi:10.1111/bre.12223. Q:50

Muñoz, J. A., J. Mencos, E. Roca, N. Carrera, O. Gratacos, O. Ferrer, and O. Fernandez, 2018, The structure of the South-Central Pyrenean fold and thrust belt as constrained by subsurface data: Geologica Acta, v. 16, no. 4, p. 439–460, doi:11.1344/GeologicaActa2018.16.4.7.

Peel, F. J., 2014, The engines of gravity-driven movement on passive margins: Quantifying the relative contribution of spreading versus gravity sliding mechanisms: Tectonophysics, v. 633, p. 126–142, doi:10.1016/j.tecto.2014.06.023. Q:51

Péron-Pinvidic, G., G. Manatschal, and "IMAGinING RIFTING" Workshop Participants, 2019, Rifted margins: State of the art and future challenges: Frontiers of Earth Science, v. 7, p. 218, doi:10.3389/feart.2019.00218.

Pichel, L. M., and C. A.-L. Jackson, 2020, The enigma of the Albian Gap: Spatial variability and the competition between salt expulsion and extension: Journal of the Geological Society, v. 177, no. 6, p. 1129–1148, doi:10.1144/jgs2020-055.

Pilcher, R. S., B. Kilsdonk, and J. Trude, 2011, Primary basins and their boundaries in the deep-water northern Gulf of Mexico: Origin, trap types, and petroleum system implications: AAPG Bulletin, v. 95, no. 2, p. 219–240, doi:10.1306/06301010004.

Ramberg, H., 1967, Gravity, deformation and the Earth's crust: London, Academic Press, 217 p.

Ramberg, H., 1981, Gravity, deformation and the Earth's crust in theory, experiments and geological application, 2nd ed.: London, Academic Press, 452 p.

Roca, E., O. Ferrer, M. G. Rowan, J. A. Muñoz, K. A. Giles, P. Arbués, and M. de Matteis, 2021, Salt tectonics and controls on halokinetic-sequence development of an exposed deepwater diapir: The Bakio Diapir, Basque-Cantabrian Basin, Pyrenees: Marine and Petroleum Geology, v. 123, 104770, 28 p., doi:10.1016/j.marpetgeo.2020.104770.

Roelofse, C., T. M. Alves, J. Gafeira, and K. O. Omosanya, 2019, An integrated geological and GIS-based method to assess caprock risk in mature basins proposed for carbon capture and storage: International Journal of Greenhouse Gas Control, v. 80, p. 103–122, doi:10.1016/j.ijggc.2018.11.007.

Rouby, D., S. Raillard, F. Guillocheau, R. Bouroullec, and T. Nalpas, 2002, Kinematics of a growth fault/raft system on the West African margin using 3-D restoration: Journal of Structural Geology, v. 24, no. 4, p. 783–796, doi:10.1016/S0191-8141(01)00108-0.

Rowan, M.G., 2004, Do salt welds seal? *in* P. J. Post, D. L. Olson, K. T. Lyons, S. L. Palmes, P. F. Harrison, and N. C. Rosen, eds., Salt sediment interactions and hydrocarbon prospectivity concepts, applications and case studies for the 21st century: Tulsa, Oklahoma SEPM Special Publication 24, p. XX–XX, doi:10.5724/gcs.04.24.0390.

Rowan, M. G., 2014, Passive-margin salt basins: Hyperextension, evaporite deposition, and salt tectonics: Basin Research, v. 26, no. 1, p. 154–182, doi:10.1111/bre.12043. Q:52

Rowan, M. G., and K. A. Giles, 2021, Passive versus active salt diapirism: AAPG Bulletin, v. 105, no. 1, p. 53–63, doi:10.1306/05212020001.

Rowan, M. G., and K. A. Giles, 2023, Different scales of salt-sediment interaction during passive diapirs: AAPG Bulletin, v. 107, no. 1, p. 7–22, doi:10.1306/0104202221069.

Rowan, M. G., K. A. Giles, T. E. Hearon IV, and J. C. Fiduk, 2016, Megaflaps adjacent to salt diapirs: AAPG Bulletin, v. 110, no. 11, p. 1723–1747, doi:10.1306/05241616009.

Rowan, M. G., F. J. Peel, and B. C. Vendeville, 2004, Gravity-driven fold belts on passive margins, *in* K. R. McClay, ed., Thrust tectonics and hydrocarbon systems.: AAPG Memoir 82, p. 157–182.

Rowan, M. G., F. J. Peel, B. C. Vendeville, and V. Gaullier, 2012, Salt tectonics at passive margins: Geology versus models – Discussion: Marine and Petroleum Geology, v. 37, no. 1, p. 184–194, doi:10.1016/j.marpetgeo.2012.04.007.

Rowan, M. G., and P. Weimer, 1998, Salt-sediment interaction, northern Green Canyon and Ewing Bank (offshore Louisiana), northern Gulf of Mexico: AAPG Bulletin, v. 82, no. 5B, p. 1155–1182.

Santolaria, P., P. Granado, N. Carrera, C. L. Schneider, O. Ferrer, M. Snidero, P. Strauss, K. Pelz, E. Roca, and J. A. Muñoz, 2021, From downbuilding to contractional reactivation of salt-sediment systems: Insights from analog modeling: Tectonophysics, v. 819, 229078, 20 p., doi:10.1016/j.tecto.2021.229078.

Sapin, F., J.-C. Ringenbach, and C. Clerc, 2021, Rifted margins classification and forcing parameters: Scientific Reports, v. 11, no. 1, 8199, 17 p., doi:10.1038/s41598-021-87648-3.

Schellart, W. P., 2000, Shear test results for cohesion and friction coefficients for different granular materials: Scaling implications for their usage in analogue modeling: Tectonophysics, v. 324, no. 1–2, p. 1–16, doi:10.1016/S0040-1951(00)00111-6.

Schellart, W. P., and V. Strak, 2016, A review of analogue modelling of geodynamic processes: Approaches, scaling, materials and quantification, with an application to subduction experiments: Journal of Geodynamics, v. 100, p. 7–32, doi:10.1016/j.jog.2016.03.009.

Schultz-Ela, D. D., 2001, Excursus on gravity gliding and gravity spreading: Journal of Structural Geology, v. 23, no. 5, p. 725–731, doi:10.1016/S0191-8141(01)00004-9.

Séguret, M., 1972, Étude tectonique des nappes et séries décollées de la partie centrale du versant sud des Pyrénées: Montpellier, France, Publications USTL, Série Géeologie Structuralle 2, XX p. Q:53

Snedden, J. W., and W. E. Galloway, 2019, The GoM sedimentary basin: Depositional evolution and petroleum applications: Cambridge, United Kingdom, Cambridge University Press, 326 p.

Souquet, P., 1967, Le Cretacé superieur sud-pyrénéenne en Catalogne, Aragon et Navarre, Ph.D. dissertation, University of Toulouse, Toulouse, France, XX p.

Strauss, P., P. Granado, and J. A. Muñoz, 2021a, Reply to the comment of Schollnberger on ‘Subsidence analysis of salt tectonics-driven carbonate minibasins’ (Northern Calcareous Alps, Austria): Basin Research, v. 33, no. 5, p. 2636–2642, doi:10.1111/bre.12577. Q:54

Strauss, P., P. Granado, and J. A. Muñoz, 2021b, Subsidence analysis of salt tectonics-driven carbonate minibasins (Northern Calcareous Alps, Austria): Basin Research, v. 33, no. 2, p. 968–990, doi:10.1111/bre.12500.

Sutra, E., G. Manatschal, G. Mohn, and P. Unternehr, 2013, Quantification and restoration of extensional deformation along the Western Iberia and Newfoundland rifted margins: Geochemistry Geophysics Geosystems, v. 14, no. 8, p. 2575–2597, doi:10.1002/ggge.20135.

Talbot, C. J., 1995, Molding of salt diapirs by stiff overburden, *in* M. P. A. Jackson, D. G. Roberts, and S. Snelson, eds., Salt tectonics: A global perspective: AAPG Memoir 65, p. 61–75.

Tavani, S., P. Granado, and F. Balsamo, 2018, Petroleum system in supra-salt strata of extensional forced-folds: A case-study from the Basque-Cantabrian basin (Spain): Marine and Petroleum Geology, v. 96, p. 315–330, doi:10.1016/j.marpetgeo.2018.06.008.

Trusheim, F., 1960, Mechanism of salt migration in northern Germany: AAPG Bulletin, v. 44, p. 1519–1540.

Tugend, J., G. Manatschal, N. J. Kusznir, E. Masini, G. Mohn, and I. Thinon, 2014, Formation and deformation of hyperextended rift systems: Insights from rift domain mapping in the Bay of Biscay Pyrenees: Tectonics, v. 33, no. 7, p. 1239–1276, doi:10.1002/2014TC003529.

Urai, J. L., Z. Schléder, C. J. Spiers, and P. A. Kukla, 2008, Flow and transport properties of salt rocks, *in* R. Littke, U. Bayer, D. Gajewski, and S. Nelskamp, eds., Dynamics of complex intracontinental basins: The Central European Basin system: Berlin, Springer Verlag, p. 277–290.

Uranga, R., O. Ferrer, G. Zamora, J. A. Muñoz, and M. G. Rowan, 2022, Salt tectonics of the offshore Tarfaya Basin, Moroccan Atlantic margin: Marine and Petroleum Geology, v. 138, p. 10552, 20 p., doi:10.1016/j.marpetgeo.2021.105521.

Vendeville, B. C., 2002, A new interpretation of Trusheim’s classic model of salt-diapir growth: Gulf Coast Association of Geological Societies Transactions, v. 52, p. 943–952.

Vendeville, B. C., 2005, Salt tectonics driven by sediment progradation: Part I - Mechanics and kinematics: AAPG Bulletin, v. 89, no. 8, p. 1071–1079, doi:10.1306/03310503063.

Vendeville, B. C., H. Ge, and M. P. A. Jackson, 2015, Scale models of salt tectonics during basement-involved extension: Petroleum Geoscience, v. 1, no. 2, p. 179–183, doi: 10.1144/petgeo.1.2.179.

Vendeville, B. C., and M. P. A. Jackson, 1992a, The fall of diapirs during thin-skinned extension: Marine and Petroleum Geology, v. 9, no. 4, p. 354–371, doi:10.1016/0264-8172(92)90048-J. Q:55

Vendeville, B. C., and M. P. A. Jackson, 1992b, The rise of diapirs during thin-skinned extension: Marine and Petroleum Geology, v. 9, no. 4, p. 331–354, doi:10.1016/0264-8172(92)90047-I.

Wagner, B. H., 2011, An analysis of salt welding, Ph.D. dissertation, The University of Texas at Austin, Austin, Texas, 236 p.

Warsitzka, M., J. Kley, and N. Kukowski, 2015, Analogue experiments of salt flow and pillow growth due to basement faulting and differential loading: Solid Earth, v. 6, no. 1, p. 9–31, doi:A10.5194/se-6-9-2015.

Warsitzka, M., P. Závada, F. Jähne-Klingberg, and P. Krzywiec, 2021, Contribution of gravity gliding in salt-bearing rift basins – A new experimental setup for simulating salt tectonics under the influence of sub-salt extension and tilting: Solid Earth, v. 12, no. 8, p. 1987–2020, doi:10.5194/se-12-1987-2021. Q:56

Weijermars, R., and H. Schmeling, 1986, Scaling of Newtonian and non-Newtonian fluid dynamics without inertia for quantitative modelling of rock flow due to gravity (including the concept of rheological similarity): Physics of the Earth and Planetary Interiors, v. 43, no. 4, p. 316–330, doi:10.1016/0031-9201(86)90021-X. Q:57

Worrall, D. M., and S. Snelson,1989, Evolution of the northern Gulf of Mexico, with emphasis on Cenozoic growth faulting and the role of salt, *in* A. W. Bally and A. R. Palmer, eds., The geology of North America: An overview: Boulder, Colorado, Geological Society of America, v. A, p. 97–138.